ARTICLES
https://doi.org/10.1038/s41551-019-0404-5
nature biomedical engineering

Structural, geometric and genetic factors predict interregional brain connectivity patterns probed by electrocorticography

Richard F. Betzel[1], John D. Medaglia[2], Ari E. Kahn[1,3], Jonathan Soffer[1], Daniel R. Schonhaut[3] and Danielle S. Bassett[1,4,5,6,7]*

Electrocorticography (ECoG) data can be used to estimate brain-wide connectivity patterns. Yet, the invasiveness of ECoG, incomplete cortical coverage, and variability in electrode placement across individuals make the network analysis of ECoG data challenging. Here, we show that the architecture of whole-brain ECoG networks and the factors that shape it can be studied by analysing whole-brain, interregional and band-limited ECoG networks from a large cohort—in this case, of individuals with medication-resistant epilepsy. Using tools from network science, we characterized the basic organization of ECoG networks, including frequency-specific architecture, segregated modules and the dependence of connection weights on interregional Euclidean distance. We then used linear models to explain variabilities in the connection strengths between pairs of brain regions, and to highlight the joint role, in shaping the brain-wide organization of ECoG networks, of communication along white matter pathways, interregional Euclidean distance and correlated gene expression. Moreover, we extended these models to predict out-of-sample, single-subject data. Our predictive models may have future clinical utility; for example, by anticipating the effect of cortical resection on interregional communication.

The functional organization of neural systems is reflected in the correlation structure of spontaneous activity recorded from neurons, neuronal populations and brain areas[1–3]. These correlations can be modelled as networks of functionally connected neural elements and analysed using tools from network science[4,5]. While functional brain networks can be constructed at any spatial scale, most applications have focused on the large-scale, where non-invasive techniques such as functional magnetic resonance imaging (fMRI), scalp electroencephalography and magnetoencephalography make it possible to estimate and analyse whole-brain networks[6]. At this scale, past studies have found that functional network organization varies systematically with cognitive state[7,8], tracks disease and development[9,10], and is specific to individuals[11,12], showing its potential for classification and diagnosis.

While large-scale network modelling has become commonplace[6], its application to electrocorticography (ECoG) data is less frequent. ECoG uses electrodes to record electrical activity with high spatiotemporal resolution at the exposed cortical surface, and remains an essential tool for seizure localization and functional mapping[13–15]. Although the number of studies investigating networks reconstructed from ECoG recordings continues to grow[16–23], the generalizability of their findings is limited due to the restricted study of epilepsy patients, incomplete brain coverage within individuals and variable electrode placement across individuals. As a result, little is known about the whole-brain organization of ECoG networks.

Mapping and characterizing the organization of ECoG functional connectivity (FC) over the entire brain would directly advance both theory and practice in neuroscience. At the most basic level, it would further our understanding of how activity is organized across the brain. Since ECoG directly records activity on the cortical surface, mapping whole-brain ECoG connectivity would serve as a point of comparison and validation for networks estimated using other non-invasive techniques[24]. Second, it facilitates comparisons with other imaging and molecular biomarkers, such as structural connectivity[25] and gene co-expression patterns[26], opening the possibility of constructing and studying cross-modal models of ECoG FC. This approach would give us a better understanding of the factors that contribute to shaping interregional patterns of ECoG FC. Finally, because ECoG already has extensive clinical and translational use, understanding its organization and function as a network could inform new phenomenological models of disease, and predictive models for interventions and outcomes[23].

Here, we address the issues of sparse and inconsistent brain coverage associated with the use of ECoG, and develop a modelling framework for constructing whole-brain, parcellation-based and band-limited FC networks through the consolidation of multisubject recordings from a cohort of individuals with medication-resistant epilepsy. We use these unique data to address two basic research questions. First, we ask whether the organization of whole-brain ECoG FC is similar to that of fMRI blood-oxygen-level-dependent (BOLD) FC. We find that ECoG FC shares a topological correspondence with networks reconstructed from fMRI BOLD, including correlated connection weights, distance and frequency dependence, as well as similar modular and system-level structures. Our second

[1]Department of Bioengineering, School of Engineering and Applied Science, University of Pennsylvania, Philadelphia, PA, USA. [2]Department of Psychology, College of Arts and Sciences, University of Pennsylvania, Philadelphia, PA, USA. [3]Department of Neuroscience, Perelman School of Medicine, University of Pennsylvania, Philadelphia, PA, USA. [4]Department of Electrical and Systems Engineering, School of Engineering and Applied Science, University of Pennsylvania, Philadelphia, PA, USA. [5]Department of Neurology, Perelman School of Medicine, University of Pennsylvania, Philadelphia, PA, USA. [6]Department of Psychiatry, Perelman School of Medicine, University of Pennsylvania, Philadelphia, PA, USA. [7]Department of Physics and Astronomy, College of Arts and Sciences, University of Pennsylvania, Philadelphia, PA, USA. *e-mail: dsb@seas.upenn.edu

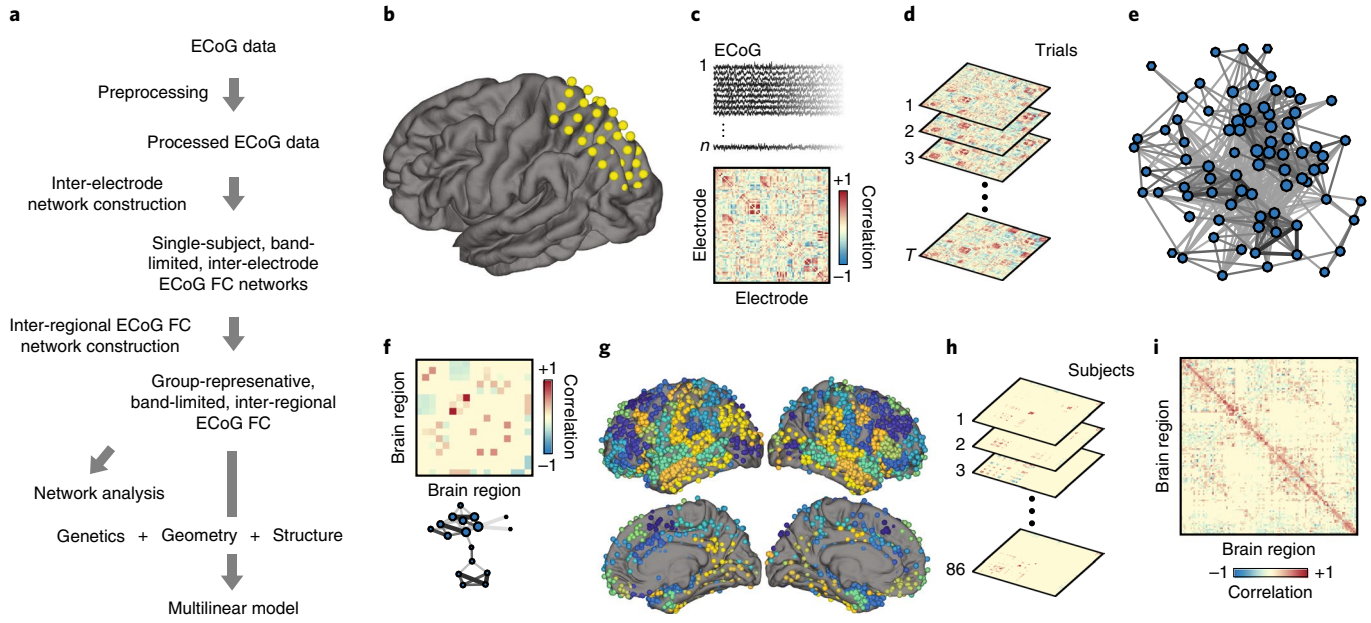

Fig. 1 | Processing pipeline for group-level ECoG FC matrices. a, Schematic showing the overall processing and analysis structure. **b**, Raw ECoG data were recorded from electrodes, the placement of which is shown by yellow circles. **c**, The recordings were preprocessed and, for each trial and frequency band, we constructed a representative correlation matrix. **d**, We extracted connections that were consistently strong across all trials. **e**, The result of this procedure was a set of single-subject, band-limited, inter-electrode ECoG FC networks. Note that in this schematic, the 'hairball' diagram of the network is plotted in an arbitrary space where nodes' (electrodes') locations are determined by a network embedding algorithm. This depiction offers a clearer view of the network's organization and heterogeneity of connections; these features are obscured and appear less salient in anatomical space due to the regular spacing of electrodes. **f**, We mapped electrode locations to vertices on the brain's surface, and subsequently to brain regions (top). This procedure resulted in an interregional ECoG FC representation (bottom) of each subject's inter-electrode network. Again, the locations of nodes (brain areas) in this layout were determined algorithmically and are not in any anatomical coordinate system. **g**, We aggregated the electrodes across the entire cohort (the colour of electrodes indicates the brain region to which they were assigned). **h**, This procedure enabled us to combine interregional FC networks to generate an estimate of whole-brain, interregional ECoG FC. **i**, From this aggregation procedure, we calculated each connection's average weight across those observations.

goal builds on our first. Given an estimate of whole-brain ECoG FC, can we identify the factors responsible for its organization and their relative contributions? To address this question, we used a multilinear model (MLM) to explain the variability in ECoG connection weights on the basis of three factors: anatomical connectivity, interregional distance and correlated gene expression patterns. We show that the most parsimonious models require multiple factors, indicating that each factor uniquely contributes to explaining the variability in ECoG FC. We also show that the performance of these models can be improved by computing gene expression correlation matrices using restricted subsets of genes. Importantly, these subsets are enriched for maintenance and regulation of ion channels and membrane potentials, suggesting genetic underpinnings of ECoG connectivity. Finally, we fit models to single-subject ECoG networks and show that the best-fitting models exhibit both a high degree of specificity (they generate the best predictions for the subject they were fit to) and a high degree of generalizability (they generate good out-of-sample predictions).

Results

Whole-brain ECoG FC networks. We analysed ECoG recordings from 86 subjects recorded during resting periods between trials of a free recall task (Fig. 1). The process of estimating whole-brain FC from these recordings involved several steps. First, ECoG data were preprocessed and filtered into 7 frequency bands (1–4, 4–8, 8–13, 13–25, 25–45, 85–115 and 140–165 Hz). For each subject and trial, we calculated the full matrix of inter-electrode correlations from the filtered time series. This matrix was then transformed into an interregional correlation matrix by mapping electrodes to $n = 114$ brain regions based on their locations in Montreal Neurological Institute (MNI) standard space[27]. Finally, interregional matrices were averaged over trials and aggregated across subjects (see Supplementary Figs. 1 and 2 for electrode and connectional coverage). This process resulted in seven band-limited and group-representative correlation matrices, $A^{\mathrm{ECoG}} \in \mathbb{R}^{n \times n}$, where each element A_{ij}^{ECoG} represented the average correlation (that is, FC) of electrodes located near region i with those located near region j. We refer to these matrices as ECoG FC throughout this report (see Methods for more details of network construction). Note that ECoG and fMRI BOLD assay the same organ (the human brain), and that FCs estimated from these different recording modalities represent complementary views of the same underlying networks.

ECoG and BOLD FC feature similar global architectures. Whole-brain FC is thought to reflect the brain's intrinsic architecture and to vary systematically with cognitive state, disease and development. While FC estimated from the fMRI BOLD signal is well studied, little is known about the architecture of whole-brain ECoG FC. From a practical perspective, it would be useful to compare BOLD and ECoG FC to better understand their shared versus unique features. We therefore compared the network organization of ECoG FC directly with that of BOLD FC (see Methods for more information on fMRI BOLD acquisition and network construction).

In Fig. 2a, we show the upper triangle of the BOLD and ECoG FC (1–4 Hz) matrices side by side. On the basis of visual inspection alone, the two matrices have some commonalities, including evidence of long-distance correlations. As a more quantitative assessment of the similarity of BOLD and ECoG FC, we computed the

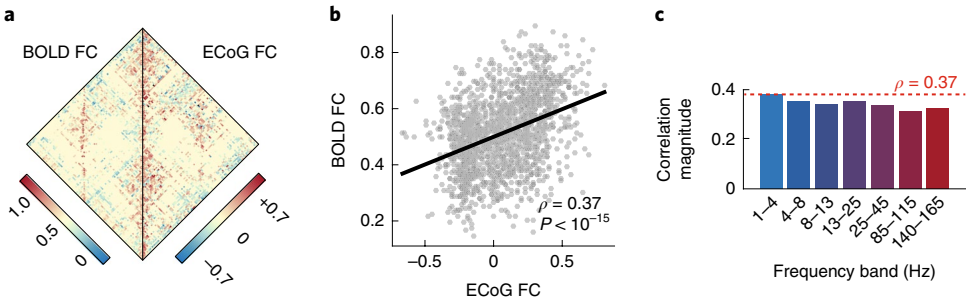

Fig. 2 | Relationship between group-level ECoG and BOLD FC. a, Side-by-side comparison of ECoG FC (1–4 Hz) and BOLD FC. **b**, Scatterplot of ECoG FC (1–4 Hz) with BOLD FC. The black line represents the best linear fit. **c**, Pearson correlation between ECoG and BOLD connectivity as a function of frequency band.

Pearson correlation coefficient between their connection weights (Fig. 2b; again, shown for the 1–4 Hz band). We note that this correlation was computed using group-composite BOLD and ECoG FC, and based on the linear relationship between 2,908 points. These points represent the set of functional connections for which we obtained an estimate of ECoG FC. We observed statistically significant correlations across all frequency bands (Fig. 2c; $P < 10^{-15}$; false discovery rate controlled at $q = 0.05$ to account for multiple comparisons). The strongest correlation was observed in the slowest frequency band (1–4 Hz; Spearman rank correlation $\rho = 0.37$; $P < 10^{-15}$; Fig. 2c), suggesting that slow, coherent fluctuations in the ECoG signal may contribute to observed patterns of BOLD FC. It is worth noting that the magnitude of the correlation between ECoG FC and BOLD FC, although statistically significant, was nonetheless quite modest.

ECoG modules overlap with functional systems. Many studies have shown that BOLD FC can be decomposed into modules of densely interconnected brain regions[28]. These modules map closely onto patterns of task-induced activations and recapitulate the brain's large-scale functional and cognitive systems[1,29]. Here, we asked whether it was possible to identify modules with similar topographical features by applying module detection algorithms to low-frequency (1–4 Hz) interregional ECoG FC, as it exhibited the strongest correlation with BOLD FC across preprocessing pipelines. To address this question, we first explored the space of possible ECoG FC modules using the well-known modularity maximization technique (see Methods)[30] (see Supplementary Fig. 3 for a schematic illustration of this procedure). This procedure generated high-quality partitions of brain regions into non-overlapping modules, which were represented as indicator vectors (the *i*th element of a vector was equal to '1' if brain region *i* belonged to that module, and was equal to '0' otherwise). Next, we computed the spatial similarity of detected modules with seven canonical brain systems corresponding to the dorsal attention, cognitive control, default mode, visual, limbic, somatomotor and salience networks[1].

Of all detected modules, approximately 80% exhibited greater-than-expected similarity to one or more brain systems ($P < 0.05$; permutation test), suggesting that there exists a broad correspondence of ECoG FC modules and brain systems. Here, similarity was calculated using the Jaccard index, and the observed value was compared against a null distribution generated by randomly and uniformly permuting module and system labels (see Methods for more details). In Fig. 3a, we show module indicator vectors grouped according to the system with which they shared the greatest similarity. In Fig. 3b, we show the average vector for each system. In addition to this quantitative analysis, we also visualized these data using two other approaches. In Fig. 3c, we show the results of a principal component analysis on the full set of indicator vectors, and we visualize the detected modules in a two-dimensional space. In this plot, each point represents a detected module whose colour measures that module's 'purity' (grey points are modules that have no clear correspondence to a brain system, whereas modules with clearer mappings to brain systems are coloured brightly). Overall, we found that modules with high similarity to a given brain system are grouped close to one another, supporting the intuition that the detected modules had a strong correspondence with known cognitive systems. Finally, we visualized a subset of the detected modules in anatomical space. We did this by identifying and averaging over the ten module indicator vectors with the greatest similarity to each cognitive system (Fig. 3d). We also show that, in general, these average vectors were uncorrelated with one another (Fig. 3e).

The correspondence of ECoG modules and canonical systems suggests that, despite differences in modality and small-scale features (for example, the precise weights of connections), much of the large-scale structure of brain network organization observed in other neuroimaging modalities from which these canonical systems can be derived is preserved in ECoG FC. Moreover, the correspondence of modules to the brain's system-level architecture suggests that low-frequency ECoG FC might be especially useful for studying cognitive processes. Nonetheless, the correspondence between ECoG FC modules and canonical systems is imperfect (note that in Fig. 3d the posterior and lateral components of the default mode are poorly recapitulated by detected modules). The presence of such differences suggests that while whole-brain ECoG FC shares many features with BOLD FC, it nonetheless offers distinct and complementary perspectives on the brain's functional architecture.

Functional connections are band specific and distance dependent. The existence of strong modular structure that maps onto well-known cognitive systems motivates the question of what other principles might explain the architecture of ECoG FC. To probe this question, we began by examining the degree to which the physical distance separating brain regions might play a role in shaping the observed FC. Specifically, we hypothesized that long-distance coordination of brain areas is supported by the correlation of frequency-specific fluctuations[31]. This effect has been previously observed in inter-electrode FC networks[32], although the extent to which it persists at the level of brain regions remains unclear. To test our hypothesis, we assessed whether the magnitude of ECoG FC was related to connection length as estimated by Euclidean distance. We observed a statistically significant inverse relationship between these two variables ($P < 10^{-15}$), indicating that the correlation magnitude of the ECoG signal within proximal regions tends to be stronger than that between distant regions, possibly as a reflection of cost and energetic constraints[33] (Fig. 4a; as examples, we show the slowest and fastest frequency bands).

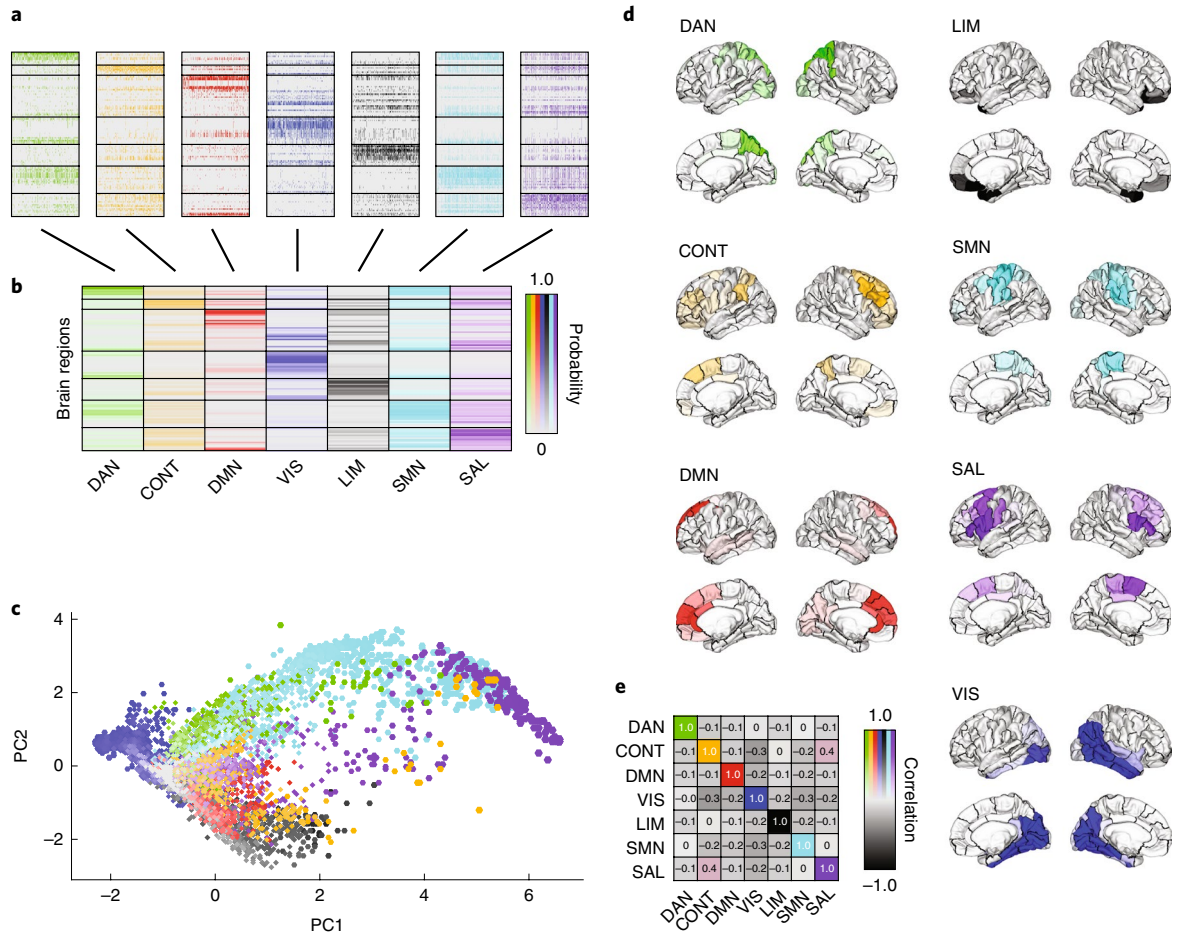

Fig. 3 | Relationship between group-level ECoG modules and canonical systems. We wished to assess whether modules detected in ECoG FC mapped onto canonical brain systems (that is, dorsal attention (DAN), control (CONT), default mode (DMN), visual (VIS), limbic (LIM), somatomotor (SMN) and salience (SAL) networks). **a**, Each block depicts indicator vectors corresponding to detected modules (based on ECoG FC in the 1–4 Hz range) and the system to which they were most similar. Rows represent brain regions (the horizontal bars divide brain systems from one another) and columns represent different detected modules. **b**, Averaging over all modules assigned to a given system produced a mean assignment vector. **c**, We also performed a principal components analysis of all detected modules. We plotted the position of each module, using as coordinates only the values of the first two components (PC1 and PC2). In general, systems were localized in this low-dimensional space, so that modules with similar system assignments appeared near one another. **d**, As visual confirmation that the detected ECoG modules were similar to brain systems, we computed the average module assignment of the top ten modules most similar to each system, and plotted these assignments back onto the cortical surface. While imperfect, these assignments bore a striking resemblance to canonical systems. **e**, Finally, we computed the Pearson correlation of mean assignment vectors for each system and found that, as expected, these vectors were largely independent of one another and uncorrelated.

The strong inverse relationship between connection weight and distance has implications for the observed modular organization of ECoG FC. For every detected module, we computed its size along with its internal density and spatial extent (mean inter-regional correlation and Euclidean distance, respectively). These last two measures served as indicators of a module's cohesiveness and anatomical distribution over the cortex. For modules of a given size, we found that slower frequencies generally exhibited stronger connection weights and broader spatial extents compared with faster-frequency bands (Fig. 4b,c). We quantified this intuition using methods from functional data analysis, which are statistical tools for comparing continuous curves[34]. Specifically, for the slowest and fastest frequency bands, we computed test statistics as the summed point-wise difference in mean internal density and spatial extent as a function of module size. We compared these observed values against a null model in which modules of the same size were randomly reassigned to frequency bands. We observed the most profound differences between the slowest three frequency bands (1–13 Hz) and the fastest four frequency bands (13–165 Hz) (average: $z = 21.5 \pm 6.5$ and corresponding $P < 10^{-15}$). This result, which is in agreement with earlier studies[31,35], suggests that high-frequency oscillations modulate local, short-range interactions, but that long-distance correlations are driven by much slower rhythms. More broadly, these findings are consistent with previous reports showing that cognitive and psychological processes are underpinned by areally and frequency-specific patterns of activity[36–38].

Predicting whole-brain ECoG FC from geometry, structure and genetics. Despite the ease with which FC can be measured and accessed experimentally, it can be viewed epiphenomenally as the product of interacting structural, geometric and genetic processes. Structural connections, such as synapses, axonal projections and fibre bundles, constrain communication patterns among neural elements, and structure the propagation of activity across the brain and its correlation patterns[25,39,40]. Factors that influence anatomical connectivity also play important, albeit indirect, roles in shaping FC.

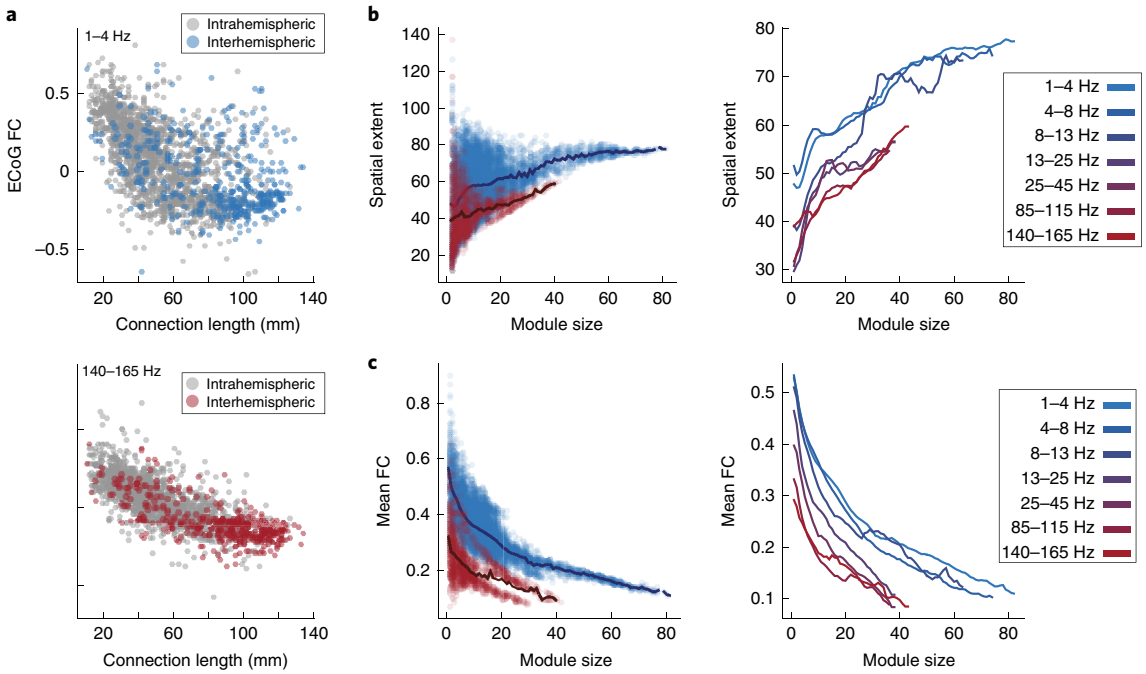

Fig. 4 | Distance dependence of ECoG FC and community properties. a, Edge weight, on average, decreases as a function of distance. We show examples for the 1–4 Hz (top) and 140–165 Hz (bottom) frequency bands. On average, slower-frequency bands exhibited a greater proportion of strong, long-distance correlations. This relationship was evident at the level of brain modules. **b**, For modules of a given size (number of nodes), slower-frequency bands tended to have a greater spatial extent (mean interregional distance). As an example, we show scatterplots (left) of the spatial extent as a function of size for modules detected using 1–4 and 140–165 Hz ECoG FC. Each point represents an individual module, and the lines represent the mean spatial extent as a function of distance. For completeness, we also show the mean spatial extent as a function of module size for all frequency bands (right). **c**, Similarly, for a given size, the module density was greater for ECoG FC computed in slower-frequency bands compared with faster-frequency bands. As an example, we compare 1–4 with 140–165 Hz (left). Again, each point represents a single module and the lines represent the mean module density as a function of size. For completeness, we also show the mean module density as a function of size for all frequency bands (right).

The brain's intrinsic geometry and its drive to reduce metabolic and material connection costs result in wiring patterns that favour short, low-cost connections over longer, more costly connections[33,41]. Similarly, genetic factors regulate dendritic arborization[42], myelin integrity[43,44] and even rhythmic oscillatory activity[45]. Understanding how these and other factors shape functional network organization remains one of the overarching goals of network neuroscience[5]. While a number of studies have investigated how they relate to BOLD FC, virtually nothing is known about the relationship of these factors to networks estimated from ECoG.

To better understand how brain structure, geometry and genetics influence ECoG FC, we investigated a set of nested MLMs that generated predictions of ECoG FC connection weights, $\hat{A}^{\mathrm{ECoG}} = [\hat{A}_{ij}^{\mathrm{ECoG}}]$. Predictions were made based on a linear combination of three predictors, each representing a different neurobiological mode capable of influencing ECoG FC: search information, $S = [S_{ij}]$, which is computed from the matrix of reconstructed white matter fibre pathways, measures the 'hiddenness' of the shortest anatomical path between region i and region j[25,46]; $D = [D_{ij}]$, the Euclidean distance between region i and region j; and $G = [G_{ij}]$, the Pearson correlation between region i and region j's gene expression profiles (averaged across two donors) (see Methods). Model performance was defined as the Pearson correlation between the ECoG FC generated by the model and the observed ECoG FC.

This modelling framework is built on the assumption that whole-brain FC, which is thought to underpin cognitive function, depends on spatial, structural and genetic factors. The relationship of spatial and structural factors to FC is intuitive—brain areas that are strongly connected structurally and/or located near one another are also likely to be connected by strong functional connections. In addition, we included a genetic factor, as gene expression levels are known to influence local cellular function[47]. In our model, and in line with recent work[26,48], we hypothesize that brain areas with similar expression profiles (and presumed similar cellular functionality) are also likely to be functionally connected to one another.

The full MLM including all three predictors is given by (Fig. 5a):

$$A^{\mathrm{ECoG}} = \beta_0 + \beta_S S + \beta_D D + \beta_G G \quad (1)$$

We tested all possible combinations of predictors, constituting seven models in total, and identified the optimal model for each frequency band based on the Akaike information criterion (AIC)[49]. For a given model, the AIC was calculated as:

$$\mathrm{AIC} = n_{\mathrm{samp}} \log\left[\frac{\mathrm{RSS}}{n_{\mathrm{samp}}}\right] + 2K \quad (2)$$

where n_{samp}, RSS and K are the total number of samples (pairs of brain regions for which ECoG FC information was available), the residual sum of squared errors and the total number of predictors (including the constant β_0), respectively. The value of n_{samp} was the same for all models, but varied with frequency band; models differed from one another only in terms of RSS and K.

The models that we consider are simple in the sense that they predict the magnitude of ECoG FC given a small set of predictors. This class of models has the distinct advantage of interpretability; since the number of predictors is small and their relationship to

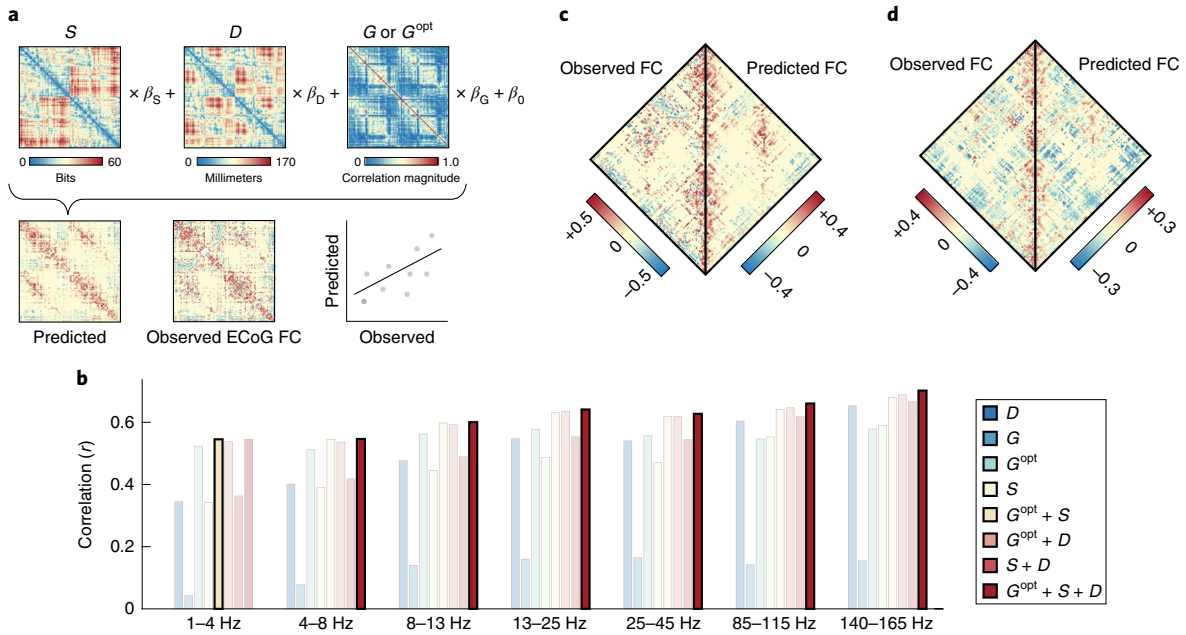

Fig. 5 | Predicting A^{ECoG} with search information, Euclidean distance and gene expression correlations. a, General structure of the MLM. Linear combinations of three predictors derived from brain structural connectivity (search information, *S*), spatial embedding (Euclidean distance, *D*) and genetics (gene expression correlation matrix or its optimized form, *G* or G^{opt}) are used to generate predictions of ECoG connectivity. The regression coefficients, β_S, β_D and β_G, are those that result in the maximum correlation between model connectivity and observed ECoG connectivity. We explore seven different combinations of predictors to identify the most parsimonious model. **b**, Correlation of modelled and observed ECoG connectivity for all seven models across all seven frequency bands. The optimal model for each frequency band (as identified by the AIC) is indicated with a black border surrounding an opaque bar; all suboptimal models are partially transparent. **c**,**d**, We show modelled and observed ECoG connectivity matrices side by side for the lowest-frequency band (**c**; 1–4 Hz) and the highest-frequency band (**d**; 140–165 Hz). The left half of each plot shows the observed pattern of ECoG FC, while the right half shows the pattern generated by the model.

ECoG FC is linear, comparing the differential contributions of each factor is straightforward and tractable. However, these models are also amechanistic and do not offer process-based and neurophysiological explanations for how structural, distance and genetic factors shape ECoG FC. In general, models of FC span a continuum from simple and predictive to mechanistic and causal. Our decision to focus on the simpler class of models is in line with recent cross-modal studies relating structural and functional imaging modalities to one another[25,39] and, critically, allows us to parse the contributions of structure, distance and genes in explaining the variability of ECoG FC connection weights.

Single-factor models. The simplest models we tested used single factors (S, D or G) to predict ECoG FC. Despite their simplicity, we found that in some cases they performed surprisingly well (Fig. 5b). Across all frequency bands, search information and Euclidean distance performed the best. The correlation of modelled and observed ECoG FC based on either of these factors never fell below $r=0.345$, and in the highest-frequency bands reached a level of $r=0.654$. In contrast, correlated gene expression consistently performed worst, achieving a maximum correlation of $r=0.156$.

These observations prompted us to pursue two additional experiments. First, because search information and Euclidean distance performed similarly, and due to ongoing debate over the role that distance plays in shaping anatomical connectivity (used to estimate search information), we wished to test whether search information generated statistically significant predictions of ECoG FC above and beyond that of Euclidean distance. As expected, we found that search information (derived from the network of white matter connections) and distance were correlated with one another ($r=0.74$; $P<10^{-15}$). To assess search information's unique contribution to ECoG FC, we partialed out the effect of distance and used the residuals to model ECoG FC. This analysis revealed that, while the overall magnitude of correlation is attenuated, the residuals nonetheless can account for some of the variance in ECoG FC (maximum *P* value (P_{max}) = ~1.3×10^{-7}; Supplementary Fig. 4). In showing a close correspondence between structural connectivity and distance, these results corroborate past studies that documented similar relationships. Also in line with past work, we show that search information (a measure based on structural connectivity) nonetheless makes a unique contribution in explaining the variability in ECoG FC connection weights beyond that of distance alone.

Second, we wished to better understand why correlated gene expression performed so poorly in explaining ECoG FC. One hypothesis is that ECoG FC has little or no genetic basis. However, past studies have refuted this hypothesis[26,48], consistently showing a non-trivial relationship between genetics and FC, although mediated by a small subsets of genes. This evidence prompted the alternative hypothesis that ECoG FC could be better explained by shifting our focus away from the correlation patterns of >10,000 genes and narrowing our focus to the correlation patterns of small groups. Because the problem of identifying such groups is computationally intractable, we resorted to numerical methods for generating estimates. Briefly, we used a simulated annealing algorithm to optimize model performance while varying the size of the gene group (from 10–360 in increments of 10) and the membership of the gene group (see Methods section 'Gene ECoG optimization' for more details; Supplementary Fig. 5). We repeated this procedure separately for all seven frequency bands. With groups of 181 ± 23 genes (mean ± s.d. across frequency bands), we found that we could dramatically improve the model performance (Fig. 5b). Improvements were greatest in the slowest-frequency band, with the performance of the

genetics single-factor model increasing from $r=0.043$ to $r=0.523$. We refer to the correlation matrix of genes' expression profiles as G^{opt}, indicating that the gene list was optimized to maximize its correspondence with ECoG FC. Note that in all subsequent analyses we use these optimized lists of genes in place of the complete list.

Multifactor models. In addition to the single-factor models, we explored increasingly complex models, which included combinations of multiple factors. Seeking a balance between a model's explanatory power and its complexity, we used the AIC to identify the most parsimonious model for each frequency band. For the slowest frequency, the optimal model included two predictors (search information and optimized gene co-expression). For all other bands, the optimal model included all three predictors (search information, Euclidean distance and optimized gene co-expression), indicating that the brain's functional architecture, when estimated as ECoG FC, is shaped by a plurality of factors (Fig. 5b). We show examples of ECoG FC generated by the model for the lowest (1–4 Hz) and highest (140–165 Hz) frequency bands (Fig. 5c,d). It should also be noted that while all models tested here were fit using connections from across the entire brain, this framework can easily be extended to the level of individual brain systems, and it can be fit based on specific subsets of connections (see Supplementary Materials section on system-level MLMs and Supplementary Figs. 6–8).

Predicting single-subject ECoG FC. To this point, we have demonstrated that ECoG FC has properties similar to BOLD FC and that, with measures based on brain structure, geometry and genetics, we can explain variability in the strength of ECoG FC between brain regions. These analyses were carried out using group-representative data, which unfortunately makes it impossible to disentangle the contributions of individual subjects. In contrast, subject-level predictive models have important clinical implications and open the possibility for predicting functional effects of neurosurgery or stimulation[50].

In the following section, we extend the group-level modelling framework to the level of single-subject data. Our aim is to show that the same factors that combine to explain variance in group-level ECoG FC are generalizable to the level of single subjects and vice versa, suggesting a common set of organizational principles acting at both levels. To achieve this aim, we show that the group-level models make good predictions of single-subject, out-of-sample ECoG FC. We also confront the more challenging task of fitting the model to incomplete, single-subject data and, with the resulting models, predicting the ECoG FC of other subjects. We find that the single-subject models exhibit stereotypical differences unique to each individual, but nonetheless remain highly generalizable and can predict the ECoG FC of other subjects. At the same time, the generalizability of group-level models indicates that ECoG FC may be organized based on a shared set of principles.

First, we tested the group-level model's robustness using a 'leave-one-subject-out' procedure in which we estimated whole-brain ECoG FC matrices using data from $n-1$ subjects (Table 1). Next, we fit the full model using these data, and used the regression coefficients to predict the ECoG FC of the left-out subject (Fig. 6a). We repeated this procedure, holding out each subject, and found that generally we could predict single-subject ECoG FC with a high degree of accuracy using the group-estimated regression coefficients. Across all frequency bands, we observed that the interquartile range of correlations between predicted and observed ECoG FC always excluded zero (Fig. 6b), showing that the MLM approach has utility in predicting subject-level ECoG FC.

Using $n-1$ subjects to fit model parameters and estimate whole-brain ECoG FC is still relatively easy; the whole-brain, interregional ECoG FC matrix contains thousands of observations used to fit the MLM, meaning that the optimal parameters are not especially biased by any single subject (which contributes to only a subset of the observations). A more challenging task is to fit the model using single-subject data, which offer far fewer observations of ECoG FC and are limited by the placement of electrode grids in terms of which interregional observations are available. Nonetheless, we tested whether models fit to individual subject's ECoG FC could be used to predict the ECoG FC of the remaining $n-1$ subjects (Fig. 6c). If so, this finding would support the hypothesis that ECoG FC is organized according to similar wiring rules across different subjects.

We found that even with far fewer observations, we were still able to make good predictions of subjects' ECoG FC using parameters estimated from other subjects' ECoG FC. As expected, the parameter fits were subject specific (that is, parameters best predicted ECoG FC of the subject whose data were used to estimate it (Fig. 6d)). Remarkably, however, the predictive capacity of these parameters did not immediately attenuate when they were applied to other subjects, with interquartile ranges excluding zero (Fig. 6d). These findings suggest excellent generalizability and the possibility that similar organizational principles explain ECoG FC network architecture across subjects. Similar to the previous sections, we observed that the predictive capacity increased with frequency (Fig. 6e), suggesting that intersubject variability may be most pronounced in slower-frequency bands.

Table 1 | Results of the 'leave-one-subject-out' procedure

	Percentile				
Frequency (Hz)	**5th**	**25th**	**50th**	**75th**	**95th**
1–4	0.212	0.391	0.522	0.654	0.795
4–8	0.208	0.407	0.550	0.638	0.794
8–13	0.158	0.478	0.602	0.696	0.800
13–25	0.263	0.565	0.650	0.703	0.853
25–45	0.269	0.575	0.649	0.716	0.818
85–115	0.330	0.582	0.705	0.789	0.860
140–165	0.378	0.635	0.751	0.827	0.887

Each row represents one of seven frequency bands. The columns represent percentiles of correlation coefficient distributions. These distributions were obtained using a 'leave-one-subject-out' procedure that entailed using the MLM fit built on data from $n-1$ subjects to predict the interregional ECoG FC of a held-out subject. The correlation coefficients measure the magnitude of the correlation between that subject's predicted and observed FC.

Gene Ontology analysis. In the previous section, we found that when we calculated the correlation of gene expression profiles across the brain using ~30,000 genes, the resulting matrix was weakly related to ECoG FC. Moreover, we found that by focusing on a small subset of genes we could dramatically improve this relationship. These findings are in line with past studies, in which the correlated expression levels of small subsets of genes (~10–100) were found to be related to patterns of BOLD FC.

One risk associated with this approach is that, due to the number of genes, it might be trivial to find a small subset whose correlated expression profiles are similar to ECoG FC. In other words, optimizing an objective function could be effectively amplifying random fluctuations in a large dataset. One way to discount this possibility is to demonstrate that the genes, which constitute the optimized list are not randomly selected and that, collectively, they comprise components of pathways that perform specific biological processes and cellular functions, or that code for cellular components. To assess such biological specificity, we performed Gene Ontology analysis on the genes comprising the optimized list. We used the software GOrilla (http://cbl-gorilla.cs.technion.ac.il) to compare the optimized list of

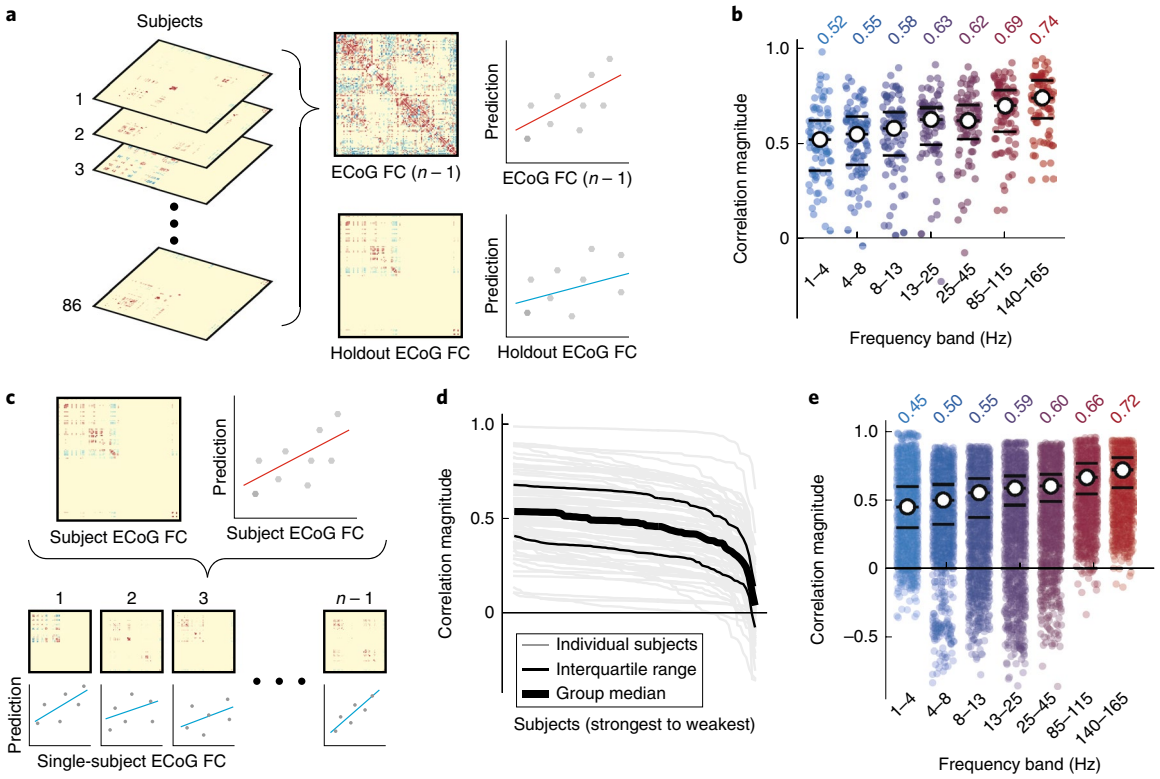

Fig. 6 | Predicting single-subject A^{ECoG}. **a**, Schematic illustrating the 'leave-one-subject-out' procedure. Models are fit using data from $n-1$ subjects to predict the FC of the remaining subject. **b**, Correlation of modelled and observed single-subject ECoG FC as a function of frequency band. Each point represents a single subject, and the total number of samples in each plot is equal to 83. **c**, Schematic illustrating the single-subject model-fitting procedure. Models are fit to data from one subject and used to predict the FC of the remaining $n-1$ subjects. **d**, Single-subject model performance. Each line represents the performance of a model fit to one of n subjects. Model performance (Pearson correlation coefficient between observed and predicted ECoG FC) is ordered from best to worst. **e**, Correlation between predicted and observed single-subject ECoG FC as a function of frequency band. The total number of samples in each box plot is $83 \times 82 = 6{,}806$. In **b** and **e**, white circles represent median values and black lines indicate interquartile ranges. Median values are also displayed numerically above the box plots.

genes against the complete list of background genes[51,52]. We focus our analysis on the slowest-frequency bands (1–4 and 4–8 Hz) because the ECoG FC generated by the linear models in these bands exhibited the greatest percentage increase as a result of replacing the co-expression matrix calculated from the full set of genes with the corresponding matrix calculated from the optimized list.

In general, the Gene Ontology analyses of both frequency bands resulted in similar findings, indicating that the optimized gene lists were enriched for biological functions related to the transport of ions across channels and cellular membranes. Near the top of both lists were ontology terms for 'sodium ion transport', 'membrane depolarization during action potential', 'monovalent inorganic cation transport', 'regulation of transport', 'sodium ion transmembrane transport' and 'sodium ion transport' ($P_{max} = 8.5 \times 10^{-4}$). Similarly, in terms of molecular function, both frequency bands were enriched for 'voltage-gated ion channel activity involved in regulation of postsynaptic membrane potential' and 'voltage-gated sodium channel activity' (P_{max} value $= 4.79 \times 10^{-4}$). Also, in terms of cellular components, the 4–8 Hz frequency band was enriched for terms related to membrane channels, including 'cation channel complex', 'voltage-gated sodium channel complex', 'ion channel complex', 'transmembrane transporter complex', 'potassium channel complex', 'transporter complex' and 'sodium channel complex' (P_{max} value $= 4.67 \times 10^{-4}$) (see Supplementary Tables 4–8 for a complete list of enriched terms).

In a previous section, we demonstrated that the correspondence of ECoG FC and patterns of correlated gene expression could be strengthened by narrowing our focus onto select subsets of genes. Here, we offer additional support to further strengthen this relationship, demonstrating that the optimized list of genes is enriched for terms associated with membrane channels and ion transport. These findings further suggest a molecular and genetic underpinning of ECoG FC.

Robustness to methodological variation. The results presented here depended on a particular sequence of decisions concerning how to process, analyse and synthesize several multimodal brain imaging datasets. To ensure their robustness, we confirmed that our results hold under reasonable variation to this sequence. Specifically, we demonstrated the consistency of ECoG FC networks with respect to variation in the distance threshold used in the electrode-to-region mapping (Supplementary Fig. 9) and using different measures of FC, namely the phase-locking value and a lagged correlation measure (Supplementary Figs. 10 and 11). We also tested variants of the MLM in which we substituted the current gene expression correlation matrix with one constructed from genes shown to be predictive of BOLD FC in a previous study (Supplementary Fig. 12 and Supplementary Table 1), and in which we substituted the current search information matrix with one estimated from a second independent structural connectivity dataset (Supplementary Fig. 13 and Supplementary Table. 2). We also fit models using a restricted subset of observations, namely the connections that were observed in all seven bands (Supplementary Table 3). In addition to methodological variation arising from the choice of parameters and processing

details, we also tested different strategies for modelling single-subject ECoG FC other than the MLM framework. Briefly, these alternative procedures included directly computing the correlation between subject- and group-level ECoG FC, assigning connections to bins according to their weight and testing whether the model recovered the correct bins, as well as separately modelling connections that were observed (included in the group ECoG FC and used to fit the model) and unobserved (present in subject-level data but not in the group matrix) (Supplementary Fig. 14). Additionally, to reduce the possibility of overfitting using our gene optimization algorithm, we repeated the MLM analysis in its entirety, including model selection, with a gene co-expression matrix calculated using genes preselected based on those identified in ref. [26] (Supplementary Fig. 15). Finally, we demonstrate that our results are not qualitatively different after correcting our estimates of ECoG FC for possible autocorrelations. We report a close correspondence between the original and corrected ECoG FC (Supplementary Fig. 16) and we still find that ECoG FC and BOLD FC exhibit their closest correspondence in the slowest (1–4 Hz) frequency band. However, we also report some diverging results; rather than a decrease in ECoG-BOLD correspondence as a function of increasing frequency, we observe a 'U-shaped' curve, with the strongest correspondence in the slowest-frequency band and the next strongest correspondence in the fastest frequency band. Details concerning these additional analyses are included in the Supplementary Materials.

Discussion

In this report we propose a technique for estimating whole-brain FC from ECoG recordings aggregated across multiple subjects. This approach facilitated the construction of (near) whole-brain, band-limited ECoG networks that parsimoniously represented the functional interactions between cortical areas as measured by co-variation in regional estimates of sensor signals. Visually, these networks displayed similar topological properties to those observed in BOLD fMRI resting-state networks—an observation that we confirmed statistically to be particularly salient in the slowest-frequency bands. We also observed modular architecture in ECoG FC that bore striking similarity to well-known cognitive systems, suggesting that whole-brain ECoG FC could be a powerful approach for probing the neural substrate underlying cognitive processes. Our analysis of whole-brain ECoG FC was complemented by additional multimodal, multilinear modelling in which we modelled the variability in the magnitude of interregional ECoG FC based on the brain's structural connectivity, its embedding in three-dimensional space, and correlations among brain regions' gene expression profiles. We found that the optimal models included multiple predictors and were able to explain nearly half of the total variance in ECoG FC weights. Moreover, the models displayed utility in predicting single-subject FC patterns but, nonetheless, exhibited subject-specific variation, indicating that they were highly generalizable but also bore the 'fingerprint' of an individual.

ECoG network architecture and its drivers. Our study builds on recent work applying network analysis to study inter-electrode ECoG FC patterns[16–20,22,23,53–55]. Whereas these past studies focused on networks where nodes represented electrodes, which are not consistent across subjects nor do they cover the whole brain, we studied interregional ECoG networks. Our effort was similar in this capacity to another recent paper[55]. Unlike the other paper, which aimed in part to relate interregional ECoG FC to cognitive measures, our focus was on characterizing the basic topological principles of ECoG FC organization and predicting connectivity patterns using simple models. Our approach is in line with other models of FC[25], although it has the distinct advantage of modelling FC derived from ECoG, which has clearer neural provenance[24] and is less influenced by motion and physiological artefacts than the BOLD signal[56]. Nonetheless, it is important to note that while ECoG and BOLD record different signatures of brain activity, they both record from the same organ and assay the same underlying networks, offering both corroborative and complementary views of their architecture. These results and the system-level analyses in the Supplementary Materials suggest that structure, geometry and genetics each play critical roles in shaping whole-brain patterns of ECoG FC, and that these roles vary across the brain and are probably system specific.

Cross-modal topological signatures of brain function. One of the hallmarks of brain networks is their structural, functional and cross-modal modular organization[28]. Modules are thought to be critical for both development and evolution by compartmentalizing brain areas that perform similar functions[57]. Much emphasis of late has been placed on modules in BOLD FC networks, whose boundaries overlap with known cognitive systems, suggesting a possible network-level correlate of psychological and cognitive processes[29]. Here, we demonstrated that interregional ECoG FC networks also exhibit modular architecture, although the overlap with cognitive systems is inexact—a finding that is in line with past studies based on scalp electroencephalography and magnetoencephalography[58,59]. An important question, then, is why the modules appear different. One possibility is that the ECoG signal carries unique information about patterns of coupling among neuronal populations. Compared with the BOLD signal, ECoG represents a more direct measure of neural activity, and with increased temporal resolution it can resolve in greater detail the boundaries of putative modules. More broadly, this mismatch re-emphasizes the brain's multiplex organization, in which brain areas are linked to one another via different connection modalities (for example, structure, correlated activity or gene expression)[60].

We also observed that the spatio-topological organization of ECoG FC varied with frequency. As a result, the association of ECoG and BOLD FC was also frequency dependent, with slower frequencies generally exhibiting stronger associations, in agreement with other recent studies of ECoG FC[61]. This finding is of particular importance, as it suggests an electrophysiological basis for BOLD FC. Nonetheless, the precise mapping of fluctuations in voltage traces and broadband power of the ECoG signal (and other electrophysiological signatures of population activity) to BOLD remains unclear, with studies reporting associations across a range of frequencies[62–65]. Future work could be directed toward teasing apart these frequency-specific contributions to both BOLD and FC in greater detail.

Basic and clinical utility of prediction. In addition to identifying factors underpinning ECoG FC, the predictive modelling framework has other advantages. Specifically, it makes predictions about the magnitude of ECoG FC between brain regions for which we have no data, complementing previous efforts developing methods to predict missing data in structural connectomes[66] and biomarker data in clinical populations[67]. This capability is a particularly useful feature for a neuroimaging technique whose coverage is inversely related to the patient's safety: greater coverage is associated with greater risk for inflammation and infection[68]. Moreover, the prediction goes beyond abstract topological predictors of missing data in complex networks[69,70] by incorporating actual physiological constraints in gene and geometry. While an important methodological contribution, these predictions also have potential clinical utility in predicting neurosurgical outcomes in future studies. For example, one could potentially simulate the effect of cortical resection as in ref. [22] by selectively 'lesioning' structural connections, thereby changing the search information matrix leading to an updated ECoG FC prediction. The new and original predictions could then be compared to identify connections whose ECoG FC magnitude is expected to increase or decrease as a consequence of the lesion.

In future work, it would be of interest to test the hypothesis that this prediction could be used as a biomarker to guide surgeries, offering an additional quantitative statistic linked to surgical outcomes; for example, to predict the effect of cortical resection. Note that the clinical utility of this approach is prospective, as the validation of this approach in a clinical context is beyond the scope of the present study.

Functional organization of the cerebral cortex. Understanding the principles that guide the functional organization of neural systems remains a major neuroscientific goal. Towards this end, we identified a set of structural, geometric and genetic factors that, collectively, explained variability in the correlation magnitude of electrical activity recorded from distant brain areas. Our findings suggest that the brain's spatial layout and large-scale structural connectivity have especially strong predictive capacity and (presumably) play important roles in determining whether the activity of two brain regions is likely to become coupled. This notion is in agreement with studies reporting distance-dependent variation of functional connections[71] and close (but not exact) correspondence of interregional correlation to the topology of the underlying structural network[40,72–74].

Interestingly, we found that gene expression correlations had the least explanatory capacity of all three factors. That interregional correlations are related, in any way, to the expression levels of specific genes and transcripts is a relatively recent finding[26], and the mechanisms by which these genetic factors can enhance or suppress the synchrony of neural activity are not well understood. One possibility is that, like gene–gene co-expression networks in which genes are connected to one another if their expression levels are correlated across samples, interregional correlations of gene expression profiles are driven by sets of functionally related genes[26,75]. Allowing for speculation, these groups of genes might perform similar functions, such as ion channel regulation, thereby shaping electrophysiological activity at a low level[76]. Indeed, studies of gene polymorphisms and variants and their role in disease have reported differences in seed-based FC (estimated from fMRI BOLD) between groups[77,78].

Another possibility is that cytoarchitectural and morphological patterning, both of which influence large-scale structural[79] and (BOLD) FC[80], are genetically regulated[81], and thereby have the capacity to influence correlated interregional electrical activity. Genetic regulation of structural covariance matrices has been reported over the course of development[82], and differential gene expression across the adult human cerebral cortex reflects the spatial distribution of cell types[83]. In the present study, we did not include an estimate of structural covariance in our predictive model and, to our knowledge, a quantitative large-scale map of cortical cytoarchitecture is unavailable. Future studies could work towards addressing these shortcomings.

Simple models of complex systems. Collectively these findings build on past investigations into the singular roles played by structure, geometry and genetics in shaping BOLD and ECoG FC[26,84]. While single-predictor models offered reasonable first approximations of ECoG FC, more complex models offered superior performance while maintaining parsimony. Interestingly, we found that the search information and Euclidean distance had much greater explanatory power than the correlation pattern of all genes' expression levels. However, we also showed that the co-expression patterns of select subsets of genes were robustly related to ECoG FC, in agreement with past studies[26,48].

The models we study here are exceedingly simple. Nonetheless, they attempt to identify the organizational principles and neurobiological factors that shape ECoG FC. These results are a natural extension of past studies that used similar techniques to model BOLD FC. However, while the BOLD signal is prone to motion[56], as well as respiratory[85] and vascular[86] artefacts, the ECoG signal is a relatively unimpeded measure of electrical activity, affording us greater confidence that the FC patterns we analyse are, indeed, of neuronal provenance.

Methodological considerations. Despite its utility, the predictive framework we develop is correlative in nature[26,87]. In contrast, the spontaneous activity of neural elements (and, by extension, FC) arises from their interactions with one another, which serve to constrain some of the observed neurophysiological dynamics[88]. A truly mechanistic model, then, is one that incorporates structure and dynamics to generate synthetic neural activity, which can then be compared with observed activity and its FC[39,40]. Future work could be directed towards incorporating both distance dependence and gene expression levels into mechanistic models.

The data that we analysed (ECoG recordings and each of the predictors) are themselves accompanied by several potential limitations. Despite aggregating recordings from many subjects, there were nonetheless pairs of brain regions for which we had no estimate of ECoG FC. This shortcoming could be addressed in the near term (for example, by defining larger brain regions) and in the long term with increased cohort size. In addition, the correlation matrices of brain regions' gene expression profiles are limited, in that they were estimated using data acquired from only two subjects[89,90]. It is therefore unclear to what extent such matrices are, in fact, representative of the average individual. There are also limitations associated with the calculation of search information, which is based on a structural network of interregional, white matter fibre bundles reconstructed from diffusion-weighted images. The reconstruction procedure is, however, susceptible to false positives and negatives[91,92]. While our use of a consistency-based, group-representative set of tracts reduces this uncertainty, advances in imaging and reconstruction techniques are necessary to mitigate its effect.

Another limitation is that the cohort studied here included subjects with medication-resistant epilepsy. While the results of our models indicate that there was a good deal of within-cohort consistency, whether our results generalize more broadly and to healthy populations remains unclear. Additionally, it should be noted that while the data aggregation process enabled us to obtain near whole-brain estimates of connectivity, it also washed over potentially meaningful intersubject variability. This variability could, in future studies, be investigated more carefully. Finally, it is worth noting that the experimental conditions under which the data were acquired were not strictly resting conditions. Specifically, ECoG data were recorded during intertrial intervals of a free recall task. While subjects were not explicitly performing the tasks, they may have been anticipating their future responses.

We have reported several features of ECoG FC that appeared to be modulated by frequency content, including the presence of long-distance correlations and the strength of association with BOLD FC. While we attribute these effects to meaningful variation in regional co-fluctuations of the ECoG signal, it is worth noting that the ECoG signal itself exhibits frequency-specific properties. Among these properties is a more or less monotonic decrease in power as a function of frequency. As a result, power tends to be greatest in the slower-frequency bands, implying that the signal-to-noise ratio in that range probably exceeds that of faster frequencies. Consequently, a possible alternative explanation for the frequency-specific modulation of ECoG FC is the variation in the signal-to-noise ratio of ECoG. Future work could investigate this possibility in greater detail.

A final limitation concerns the use of the Pearson correlation as a measure of both ECoG and BOLD FC. FC is always defined loosely as a statistical association of activity recorded from distinct neural elements or locations. The number of measures that satisfy this criteria is quite large. In fact, there are many examples in the literature where measures of coherence[93], mutual information[94],

phase-locking[95], synchronization likelihood[96] and others have been used to measure the strength of FC[97]. Despite this wide range of possibilities, the most common choice remains the Pearson correlation. Because we aimed to maintain continuity with previous literature, because it is infeasible to compare all measures of FC and because we already compared three of the more popular measures, we did not consider computing FC based on fluctuations in broadband power. Future work can be directed to investigate the relative advantages and disadvantages of alternative FC metrics in studying ECoG data.

Outlook

In summary, we present a methodological framework for aggregating single-subject ECoG FC into a cohesive, whole-brain network. Our work opens the door for future studies to move beyond inter-electrode networks and investigate properties of interregional FC in ECoG, ultimately documenting how it is modulated with cognitive state and altered in disease. We further show that ECoG FC may be underpinned by a combination of structural, geometric and genetic factors, and that the contributions made by these factors are relatively consistent across individuals, suggesting a common set of organizational principles.

Methods

Functional network reconstruction. *Subject-specific, inter-electrode ECoG FC.* We analysed ECoG recordings from 86 subjects with medication-resistant epilepsy (83 of whom had usable data) who were performing multiple trials of a 'free recall' experiment (mean ± s.d. number of trials = 41.9 ± 25.6). Research protocols were approved by the institutional review boards of the participating centres and hospitals (Columbia University, Dartmouth College, Emory University, Thomas Jefferson University, Mayo Clinic, National Institutes of Health, University of Texas Southwestern, Lawrence Livermore National Laboratory and University of Pennsylvania), and informed consent was obtained from all participants and guardians. In this experiment, subjects were presented with a list of words and were later asked to recall as many as possible from the original list. Rather than focus on word presentation or recall periods, we analysed recordings during the intertrial intervals when subjects were given no explicit cognitive task. This task-free or quasi-resting state is common in analysis of fMRI BOLD data, where the correlation structure of whole-brain spontaneous activity is organized into subnetworks that reflect the brain's functional systems[98]. Specifically, we extracted 10 s of ECoG recordings (epochs) before the beginning of each trial. All ECoG data were resampled to 512 Hz. Artefactual channels were discarded, and the remaining channels were referenced to the average signal, prewhitened by retaining the residuals after fitting a first-order autoregressive model to the referenced time series, stop-filtered to remove line noise and its harmonics, and filtered into canonical frequency bands of 1–4, 4–8, 8–13, 13–25, 25–45, 85–115 and 140–165 Hz. To reduce boundary effects and to help ensure stationarity, we discarded 2.5 and 5.0 s of data from the beginning and end of each window, resulting in a 2.5 s epoch. For each subject and each trial, we computed inter-electrode FC as a zero-lag Pearson correlation[99–101]. Note that we explore other FC measures in the Supplementary Material, specifically the subsection entitled 'Alternative measures of FC'. Pairs of electrodes whose correlation magnitude was inconsistent across trials (that is, the interquartile range included a value of zero) were excluded from subsequent analyses. We retained those correlations that maintained a consistent sign across trials and therefore were more likely to be representative of the brain's intrinsic functional architecture rather than task-induced fluctuations.

Mapping electrodes to the cortical surface. Electrode locations were manually digitized using OsiriX software[102] and stored as voxels in each subject's native coordinate space. These locations were subsequently mapped to the MNI standard coordinate system using the FSL function img2stdcoord. We compared each electrode's location in MNI space with points (vertices) on the fsaverage pial surface, and assigned each vertex to an electrode if the Euclidean distance between the two was $\leq d$ mm. In the main text, we focus on the case where $d = 3$ mm, but we explore $d = 1$, 2, 4 and 5 in the Supplementary Material (Supplementary Figs. 17 and 18). Each surface vertex was also assigned to one of $n = 114$ brain regions according to an atlas[27], thereby making it possible to map electrodes to brain regions. We show single-subject electrode-to-surface mappings in Supplementary Fig. 1.

Group-representative, interregional ECoG FC. For every pair of brain regions (i and j) and each subject independently, we identified all electrode pairs, u and v, where electrode u was assigned to region i and electrode v was assigned to region j, and we estimated their average connection weights, generating a subject-specific interregional ECoG FC matrix. We estimated the connection weight, A_{ij}^{ECoG}, in the group-representative matrix as the average connection weight over all subjects. We repeated this procedure for each of the seven frequency bands, resulting in band-limited, whole-brain, interregional ECoG FC matrices. In general, because of the finite number of subjects and limited cortical coverage, the whole-brain connectivity matrices still included pairs of regions for which we had no observed connectivity data. The fraction of observed connections varied across frequency bands. In order of frequency band, starting with the slowest, these fractions were 45.2, 47.0, 45.0, 45.0, 47.3, 54.6 and 60.9% (note that these fractions are with $d = 3$ mm). Note that the synthesis of multisubject ECoG data to generate a whole-brain estimate of interregional ECoG FC is a non-standard procedure. To our knowledge, this procedure has been performed in only one other instance[55].

Group-representative, interregional correlation matrix of gene expression profiles. The correlation matrix of brain regions' gene expression profiles was reconstructed using a similar approach. We downloaded normalized microarray data from the Allen Brain Institute (http://human.brain-map.org/static/download)[83,89,90]. The full dataset includes 6 donor brains (aged 18–68 years) for which spatially mapped microarray data were obtained (~60,000 RNA probes). We focused on donors 10,021 and 9,861, which included samples (893 and 946 sites, respectively) from both the left and right hemispheres. Subsequently, we retained only those samples that were located in the cerebral cortex. Next, we extracted expression profiles for each sample, averaged over duplicate genes, and standardized expression levels across samples as z scores. The standardized measure of any sample was used to assess the extent to which a particular gene was differentially expressed at that cortical location relative to the other cortical locations in both hemispheres.

In addition to microarray data, the Allen Brain Institute also provided coordinates representing the location in MNI coordinates where each sample was collected. This information facilitated the mapping of sample sites to brain regions in a procedure exactly analogous to our approach for mapping ECoG electrodes. As a result, we obtained representative expression profiles for each brain region (provided that there were nearby samples). For each of the two donor brains, we calculated the region-by-region correlation matrix of standardized expression profiles. Due to the overall density of the whole-brain sampling, we were able to generate an estimate of gene expression correlation (a measure of similarity) for 6,286 of 6,441 possible region pairs (~97.6%).

Note that in the absence of a specific hypothesis about which genes were of particular relevance, we included all genes in our construction of the initial correlation matrices. In 'Variants of the gene expression correlation matrix' in the Supplementary Material, we follow[26] and construct correlation matrices using the same procedures as those described above, but focusing on subsets of genes identified in that paper. For our procedures related to identifying the set of genes that optimized the prediction of ECoG FC, see section 'Gene ECoG optimization' in the Methods.

Diffusion spectrum image (DSI) connectome data. We analysed a group-representative, whole-brain structural connectivity network or connectome generated by combining single-subject data from a cohort of 30 healthy adult participants. Each participant's network was reconstructed from DSIs in conjunction with state-of-the-art tractography algorithms to estimate the location and strength of large-scale interregional white matter pathways. Study procedures were approved by the Institutional Review Board of the University of Pennsylvania, and all participants provided informed consent in writing. Details of the acquisition and reconstruction have been described elsewhere[103–105]. We studied a division of the brain into $n = 114$ cortical regions[27]. On the basis of this division, we constructed for each individual an undirected and weighted connectivity matrix, $A \in \mathbb{R}^{n \times n}$, whose edge weights were equal to the number of streamlines detected between region i and region j, normalized by the geometric mean of their volumes: $A_{ij} = \frac{S_{ij}}{\sqrt{(V_i V_j)}}$

The resulting network was undirected; that is, $A_{ij} = A_{ji}$. These individual-level networks were then aggregated to form a group-representative network. This procedure can be viewed as a distance-dependent consistency thresholding of connectome data, and the details have been described elsewhere[104,106]. The resulting group-representative network has the same number of binary connections as the average individual and the same edge-length distribution. This type of non-uniform consistency thresholding has been shown to be superior to other, more commonly used forms[107]. Note that the construction of structural brain networks from diffusion imaging data using tractography is a fairly standardized process, and is the only procedure for mapping white matter fibre tracts non-invasively[108].

fMRI BOLD data. fMRI BOLD images were acquired during the same scanning session as the DSI data on a 3.0 T Siemens Tim Trio whole-body scanner with a whole-head elliptical coil by means of a single-shot gradient-echo T2* (repetition time = 1,500 ms; echo time = 30 ms; flip angle = 60°; field of view = 19.2 cm; resolution 3 mm × 3 mm × 3 mm). Preprocessing was performed using FEAT version 6.0 (fMRI Expert Analysis Tool)[109]. Images underwent the following preprocessing steps: skull-stripping with BET, motion correction with MCFLIRT (FMRIB's Linear Image Registration Tool[109]), slice timing correction (interleaved),

spatial smoothing with a 6 mm 3D Gaussian kernel, and high-pass temporal filtering to reduce low-frequency artefacts. We also performed EPI unwarping with fieldmaps to improve subject registration to standard space. Images were transformed to a standard template using FSL's affine registration tool FLIRT[109]. Subject-specific images were co-registered to their corresponding anatomical images with Boundary Based Registration[110] and subsequently registered to the standard MNI-152 structural template via a 12-parameter linear transformation. Lastly, participants' individual anatomical images were segmented into grey matter, white matter and CSF using the binary segmentation function of FAST version 4.0 (FMRIBs Automated Segmentation Tool[111]). White matter and CSF masks for each participant were then transformed to native functional space and average time series were extracted. Images were spatially smoothed using a kernel with a full width at half maximum of 6 mm. These values were used as confound regressors on our time series, along with 18 translation and rotation parameters, as estimated by MCFLIRT[112].

The average time course for each of the 114 cortical regions was extracted, and whole-brain, interregional BOLD FC was computed as the Pearson correlation among all region pairs. Note that the global signal was not regressed out of regional time series, as past studies have shown that the global signal contains neurophysiologically and behaviourally relevant information (for example, tracking relative states of arousal)[113,114]. The full matrix was subsequently averaged across all subjects to obtain a group-representative estimate (although this averaging procedure can sometimes introduce unwanted biases at the group level[115]). We denote this BOLD FC matrix as A^{BOLD}. Note that, as with the network construction from diffusion imaging data, the process of estimating FC from fMRI BOLD data is fairly standardized and widely used.

Network statistics. *Modularity maximization.* Real-world networks can be partitioned into node-level clusters called modules by selecting the cluster assignments that optimize a particular objective function. The most popular class are modularity functions, which measure the total within-module weight of connections minus that which would be expected by chance[30]. Maximizing modularity, which results in an estimate of network modules, begins by first defining a modularity matrix, B, whose elements are given by $B_{ij}=A_{ij}-P_{ij}$, where A_{ij} and P_{ij} are, respectively, the observed and expected weights between nodes i and j. Given B and a classification of each node into one of K modules, $\sigma_i \in \{1, \ldots, K\}$, we can define modularity to be:

$$Q=\sum_{ij} B_{ij}\delta(\sigma_i\sigma_j) \tag{3}$$

Maximizing modularity is accomplished by assigning nodes to communities so that as many positive elements of B fall within modules as possible.

Here, we set $B_{ij}=A_{ij}^{\mathrm{ECoG}}-\gamma C_{ij}$, where γ is a free parameter and C_{ij} is equal to either 1 or 0 depending on whether a connection was or was not observed between nodes i and j. We adopted this formulation for two reasons. First, it means that in effect the null model for existing connections is simply a constant free parameter, γ, whose value can be tuned to detect smaller or larger modules[116]. Second, it ignores pairs of nodes for which no connectivity data were available and sets their values in the modularity matrix to 0. In this way, those elements neither increase nor decrease the objective function, Q, and therefore have minimal influence on the detected modules.

Rather than focus on 'definitive' modules obtained with a single-resolution parameter, we used a sampling procedure to obtain estimates of differently sized modules by varying γ over a range from 0 to max(A), where max(A) is the largest observed interregional correlation across all frequency bands. Between these extremes, we selected 99 additional values of γ corresponding to the 1st through 99th percentiles of interregional correlation values. Next, we iterated over all 101 values of γ, obtaining a partition at each value, extracting the modules within that partition and aggregating the unique modules. We repeated this procedure until sequential repetitions uncovered less than 1% of new modules. We repeated the full procedure independently for ECoG FC estimated from each frequency band, detecting 8,075, 7,948, 2,872, 1,122, 958, 1,359 and 1,451 modules in the 1–4, 4–8, 8–13, 13–25, 25–45, 85–115 and 140–165 Hz bands, respectively.

Note that whereas the broader modularity maximization framework is used frequently in network neuroscience applications[28], our modification to make the modularity equation compatible with networks containing unobserved connections is new. In addition, the module sampling procedure described above is also non-standard; the typical approach involves fixing γ at a single value, optimizing modularity and using heuristics to identify a single 'representative' set of modules. Our approach allows us to explore a wide range of modules, making it possible to characterize their variability, and also to study modules of different sizes[117].

Module and system overlap. We assessed the similarity of modules detected using modularity maximization and canonical cognitive systems with an overlap score. Let $\mathbf{x}=[x_1, \ldots, x_n]$ be a binary module vector whose element x_i is equal to 1 if region i is assigned to that module, and 0 otherwise. Similarity, let $\mathbf{y}=[y_1,\ldots,y_n]$ be a binary system vector whose element y_i is equal to 1 if region i is assigned to that system, and 0 otherwise. The overlap of $\mathbf{x}$ and $\mathbf{y}$ is given by $s(\mathbf{x},\mathbf{y})=\frac{|\mathbf{x}\cap\mathbf{y}|}{|\mathbf{x}\cup\mathbf{y}|}$, and the standardized version of this measure is:

$$z(\mathbf{x},\mathbf{y})=\frac{s(\mathbf{x},\mathbf{y})-\mu}{\sigma}, \tag{4}$$

where μ and σ are the mean and standard deviation of $s(\mathbf{x},\mathbf{y})$ estimated by randomly permuting the elements of $\mathbf{x}$ and $\mathbf{y}$ (1,000 repetitions). Large and positive values of $z(\mathbf{x},\mathbf{y})$ therefore indicate greater overlap than expected by chance, given the module's and system's sizes. For convenience, each module was assigned to the system with which it exhibited the greatest standardized overlap.

Each module was associated with seven overlap scores (one to each of the seven systems): $S=[s_1, \ldots, s_7]$, where s_i is the overlap of the module with the ith system. The purity of that module quantifies the extent to which it overlaps with many systems (low purity) or few systems (high purity). We define module purity by first normalizing S so that its elements sum to 1. Then, we compute an entropy over these elements as purity $=-\sum_i s_i' \log_2[s_i']$, where s_i' is the normalized overlap of a module with the ith system.

Search information. Anatomical connectivity matrices obtained from diffusion imaging data and reconstructed using deterministic tractography are usually sparse, meaning that only a fraction of all possible connections exist[87,118]. Rather than use the sparse connectivity matrix to model ECoG FC, we generated a full matrix, S, whose element S_{ij} indicates the information (in bits) required to follow the shortest path from node i to node j[46]. Let $\pi_{s\to t}=\{A_{si}, A_{ij}, \ldots, A_{kt}\}$ be the series of structural edges that are traversed along the shortest path from a source node, s, to a different target node, t, and let $\Omega_{s\to t}=\{s, i, j, \ldots, k, t\}$ be the sequence of nodes along the same path. The probability of following this path under random walk dynamics is given by $P(\pi_{s\to t})=\prod_{i\in\Omega^*_{s\to t}}\frac{\pi^{(1)}_{i\to t}}{s_i}$, where $s_i=\sum_j A_{ij}$ is the weighted degree of node i, $\pi^{(1)}_{i\to t}$ is the first edge on the shortest path from node i to node t, and $\Omega^*_{i\to t}=\{s, i, j, \ldots, k\}$ is the shortest path node sequence excluding the target node. The amount of information (in bits) required to access this shortest path, then, is given by $S(\pi_{s\to t})=\log_2[P(\pi_{s\to t})]$. We can treat every pair of nodes $\{i, j\}$ as the source and target, respectively, and (provided that there exists a unique shortest path from node i to node j) we can compute $S(\pi_{i\to j})$ for all such pairs. The resulting matrix, S, termed 'search information', has been shown to be a good predictor of BOLD FC[25] and may be modulated in certain neurological disorders[119].

Network null model. We counted the number of jointly strong and long connections for ECoG FC networks that represented different frequency bands. In Fig. 2g,h, we compared those counts across frequency bands. To demonstrate the statistical significance of these findings, we also compared counts for random networks generated under a particular null model. This null model preserved the binary topology and spatial embedding of each frequency-specific network, but otherwise scrambled edge weights across frequencies. Given a pair of nodes i and j whose connection weights across frequency bands are specified by A_{ij}^f, where $f=\{1,\ldots,7\}$, we generated random networks by randomly permuting the order of those weights across frequencies and repeating this process for all pairs of nodes. It was sometimes the case that for certain pairs of nodes a connection was only observed in a subset of frequencies. In this event, the permutation was only carried out over those frequency bands in which the connection was observed.

Gene ECoG optimization. In the main text, we briefly describe a procedure for identifying genes that are related to ECoG FC. In general, we sought the list of K genes, $\Gamma^K=\{g_1, \ldots, g_K\}$ whose brain-wide co-expression matrix was maximally correlated with ECoG FC. While the exact solution of this optimization problem is computationally intractable (the full list included 29,130 genes), we could define an objective function and use numerical methods to obtain an approximate solution.

The objective function we sought to minimize was defined as follows. Let $G_1(\Gamma)$ and $G_2(\Gamma)$ be the gene co-expression matrices for each of the two donor brains calculated using the gene list, Γ. We can then vectorize each matrix by extracting its upper triangle of non-zero elements and, after doing the same for the ECoG FC matrix, A^{ECoG}, we calculate the correlation of gene expression with ECoG FC, resulting in two correlation coefficients ρ_1 and ρ_2. In general, we want the magnitudes of ρ_1 and ρ_2 to be as large as possible. Accordingly, we defined our objective function to be $F(\rho_1, \rho_2)=\min(\rho_1, \rho_2)$, so that the correspondence of any gene list, Γ, with ECoG FC is only as good as the worse of the two donor brain correlations.

As noted earlier, optimizing this function exactly is intractable, so we used a simulated annealing algorithm to generate estimates of the solution. In general, simulated annealing works by proposing initial estimates of the solution (that are usually poor), making small changes to these estimates and evaluating whether or not these changes improve the estimate. The algorithm begins in a 'high-temperature' phase, during which even changes that result in inferior estimates can be accepted, making it possible to explore the landscape of possible solutions. Gradually, a temperature parameter is reduced so that in later phases only solutions that result in improvements are accepted.

In our case, the algorithm was initialized with a temperature of $t_0=2.5$ and a randomly generated list of K genes, Γ, which represented our initial estimate of

the solution. From this list, we constructed matrices $G_1(\Gamma)$ and $G_2(\Gamma)$, calculated ρ_1 and ρ_2, and then evaluated the objective function, $F(\rho_1, \rho_2)$. With each iteration, the temperature was reduced slightly ($t_i = t_{i-1} \times 0.99975$) and one gene randomly selected from Γ was replaced with a new gene. We then used this new list, Γ', to construct $G_1(\Gamma)'$ and $G_2(\Gamma)'$, from which we eventually obtained a new value of the objective function, $F(\rho_1', \rho_2')$. If $F(\rho_1', \rho_2') > F(\rho_1, \rho_2)$, we replaced Γ with Γ' and the algorithm proceeded to the next iteration. Otherwise, we accepted the Γ' with probability $\exp\left(-\frac{[F(\rho_1,\rho_2) - F(\rho_1',\rho_2')']}{t_i}\right)$, where t_i is the temperature at the current iteration. The algorithm continued for either 200,000 total iterations or 10,000 consecutive iterations with no change in Γ.

The result of simulated annealing will usually vary somewhat from run to run. Accordingly, we repeated the algorithm 50 times. We also varied the number of genes, K, from 10–360 in increments of 10. We chose the optimal K to be the value at which the objective function was on average greatest over the 50 repetitions. Rather than treat any of the 50 estimated solutions as representative, we calculated how frequently each gene appeared across the ensemble of all 50 solutions, and we compared this frequency with what we would expect in 50 samples of K genes. We retained only those genes that appeared more frequently than expected (the false discovery rate was controlled at $q = 0.05$). These genes represented the 'optimized list' and were submitted to the ontology analysis.

Reporting Summary. Further information on research design is available in the Nature Research Reporting Summary linked to this article.

Data availability

The main data supporting the results of this study are available within the paper and its Supplementary Information files. All source data collected from the subjects are available on request via http://memory.psych.upenn.edu/RAM_Public_Data.

Code availability

All code is available from the authors upon reasonable request.

Received: 2 January 2018; Accepted: 15 April 2019;
Published online: 27 May 2019

References

1. Yeo, B. T. et al. The organization of the human cerebral cortex estimated by intrinsic functional connectivity. *J. Neurophysiol.* **106**, 1125–1165 (2011).
2. Mann, K., Gallen, C. L. & Clandinin, T. R. Whole-brain calcium imaging reveals an intrinsic functional network in *Drosophila*. *Curr. Biol.* **27**, 2389–2396 (2017).
3. Avitan, L. et al. Spontaneous activity in the zebrafish tectum reorganizes over development and is influenced by visual experience. *Curr. Biol.* **27**, 2407–2419 (2017).
4. Bullmore, E. & Sporns, O. Complex brain networks: graph theoretical analysis of structural and functional systems. *Nat. Rev. Neurosci.* **10**, 186–198 (2009).
5. Bassett, D. S. & Sporns, O. Network neuroscience. *Nat. Neurosci.* **20**, 353–364 (2017).
6. Stam, C. J. & Reijneveld, J. C. Graph theoretical analysis of complex networks in the brain. *Nonlinear Biomed. Phys.* **1**, 3 (2007).
7. Shirer, W. R., Ryali, S., Rykhlevskaia, E., Menon, V. & Greicius, M. D. Decoding subject-driven cognitive states with whole-brain connectivity patterns. *Cereb. Cortex* **22**, 158–165 (2012).
8. Cole, M. W., Bassett, D. S., Power, J. D., Braver, T. S. & Petersen, S. E. Intrinsic and task-evoked network architectures of the human brain. *Neuron* **83**, 238–251 (2014).
9. Fornito, A., Zalesky, A. & Breakspear, M. The connectomics of brain disorders. *Nat. Rev. Neurosci.* **16**, 159–172 (2015).
10. Zuo, X.-N. et al. Human connectomics across the life span. *Trends Cogn. Sci.* **21**, 32–45 (2017).
11. Finn, E. S. et al. Functional connectome fingerprinting: identifying individuals using patterns of brain connectivity. *Nat. Neurosci.* **18**, 1664–1671 (2015).
12. Gordon, E. M. et al. Individual-specific features of brain systems identified with resting state functional correlations. *NeuroImage* **146**, 918–939 (2017).
13. Voytek, B. et al. Oscillatory dynamics coordinating human frontal networks in support of goal maintenance. *Nat. Neurosci.* **18**, 1318–1324 (2015).
14. Jacobs, J. et al. Direct electrical stimulation of the human entorhinal region and hippocampus impairs memory. *Neuron* **92**, 983–990 (2016).
15. Branco, M. P. et al. Decoding hand gestures from primary somatosensory cortex using high-density ECoG. *NeuroImage* **147**, 130–142 (2017).
16. Ortega, G. J., Sola, R. G. & Pastor, J. Complex network analysis of human ECoG data. *Neurosci. Lett.* **447**, 129–133 (2008).
17. Kramer, M. A. et al. Coalescence and fragmentation of cortical networks during focal seizures. *J. Neurosci.* **30**, 10076–10085 (2010).
18. Chu, C. J. et al. Emergence of stable functional networks in long-term human electroencephalography. *J. Neurosci.* **32**, 2703–2713 (2012).
19. Wilke, C., Worrell, G. & He, B. Graph analysis of epileptogenic networks in human partial epilepsy. *Epilepsia* **52**, 84–93 (2011).
20. Burns, S. P. et al. Network dynamics of the brain and influence of the epileptic seizure onset zone. *Proc. Natl Acad. Sci. USA* **111**, E5321–E5330 (2014).
21. Keller, C. J. et al. Corticocortical evoked potentials reveal projectors and integrators in human brain networks. *J. Neurosci.* **34**, 9152–9163 (2014).
22. Khambhati, A. N., Davis, K. A., Lucas, T. H., Litt, B. & Bassett, D. S. Virtual cortical resection reveals push–pull network control preceding seizure evolution. *Neuron* **91**, 1170–1182 (2016).
23. Proix, T., Bartolomei, F., Guye, M. & Jirsa, V. K. Individual brain structure and modelling predict seizure propagation. *Brain* **140**, 641–654 (2017).
24. Dringenberg, H. C. & Vanderwolf, C. H. Involvement of direct and indirect pathways in electrocorticographic activation. *Neurosci. Biobehav. Rev.* **22**, 243–257 (1998).
25. Goñi, J. Resting-brain functional connectivity predicted by analytic measures of network communication. *Proc. Natl Acad. Sci. USA* **111**, 833–838 (2014).
26. Richiardi, J. et al. Correlated gene expression supports synchronous activity in brain networks. *Science* **348**, 1241–1244 (2015).
27. Cammoun, L. et al. Mapping the human connectome at multiple scales with diffusion spectrum MRI. *J. Neurosci. Methods* **203**, 386–397 (2012).
28. Sporns, O. & Betzel, R. F. Modular brain networks. *Annu. Rev. Psychol.* **67**, 613–640 (2016).
29. Power, J. D. et al. Functional network organization of the human brain. *Neuron* **72**, 665–678 (2011).
30. Newman, M. E. J. & Girvan, M. Finding and evaluating community structure in networks. *Phys. Rev. E* **69**, 026113 (2004).
31. Kopell, N., Ermentrout, G. B., Whittington, M. A. & Traub, R. D. Gamma rhythms and beta rhythms have different synchronization properties. *Proc. Natl Acad. Sci. USA* **97**, 1867–1872 (2000).
32. Menon, V. et al. Spatio-temporal correlations in human gamma band electrocorticograms. *Electroencephalogr. Clin. Neurophysiol.* **98**, 89–102 (1996).
33. Bullmore, Ed & Sporns, O. The economy of brain network organization. *Nat. Rev. Neurosci.* **13**, 336–349 (2012).
34. Ramsay, J. O. & Silverman, B. W. *Applied Functional Data Analysis: Methods and Case Studies* (Springer, 2002).
35. Fries, P. A mechanism for cognitive dynamics: neuronal communication through neuronal coherence. *Trends Cogn. Sci.* **9**, 474–480 (2005).
36. Muller, L. et al. Spatial resolution dependence on spectral frequency in human speech cortex electrocorticography. *J. Neural Eng.* **13**, 056013 (2016).
37. Swann, N. et al. Intracranial EEG reveals a time- and frequency-specific role for the right inferior frontal gyrus and primary motor cortex in stopping initiated responses. *J. Neurosci.* **29**, 12675–12685 (2009).
38. Watrous, A. J., Tandon, N., Conner, C. R, Pieters, T. & Ekstrom, A. D. Frequency-specific network connectivity increases underlie accurate spatiotemporal memory retrieval. *Nat. Neurosci.* **16**, 349–356 (2013).
39. Honey, C. J. et al. Predicting human resting-state functional connectivity from structural connectivity. *Proc. Natl Acad. Sci. USA* **106**, 2035–2040 (2009).
40. Adachi, Y. et al. Functional connectivity between anatomically unconnected areas is shaped by collective network-level effects in the macaque cortex. *Cereb. Cortex* **22**, 1586–1592 (2011).
41. Betzel, R. F. et al. Generative models of the human connectome. *NeuroImage* **124**, 1054–1064 (2016).
42. Bernard, D. et al. A long nuclear-retained non-coding RNA regulates synaptogenesis by modulating gene expression. *EMBO J.* **29**, 3082–3093 (2010).
43. Chiang, M.-C. et al. Genetics of brain fiber architecture and intellectual performance. *J. Neurosci.* **29**, 2212–2224 (2009).
44. Kochunov, P. et al. Genetic analysis of cortical thickness and fractional anisotropy of water diffusion in the brain. *Front. Neurosci.* **5**, 120 (2011).
45. Salmela, E. et al. Evidence for genetic regulation of the human parieto-occipital 10-Hz rhythmic activity. *Eur. J. Neurosci.* **44**, 1963–1971 (2016).
46. Rosvall, M., Grönlund, A., Minnhagen, P. & Sneppen, K. Searchability of networks. *Phys. Rev. E* **72**, 046117 (2005).
47. Arnatkeviciute, A., Fulcher, B. D. & Fornito, A. A practical guide to linking brain-wide gene expression and neuroimaging data. *NeuroImage* **189**, 353–367 (2019).
48. Krienen, F. M., Yeo, B. T., Ge, T., Buckner, R. L. & Sherwood, C. C. Transcriptional profiles of supragranular-enriched genes associate with corticocortical network architecture in the human brain. *Proc. Natl Acad. Sci. USA* **113**, E469–E478 (2016).
49. Akaike H. in *Selected Papers of Hirotugu Akaike* (eds Parzen, E. et al.) 199–213 (Springer, 1998).

50. Ezzyat, Y. et al. Direct brain stimulation modulates encoding states and memory performance in humans. *Curr. Biol.* **27**, 1251–1258 (2017).
51. Eden, E., Lipson, D., Yogev, S. & Yakhini, Z. Discovering motifs in ranked lists of DNA sequences. *PLoS Comput. Biol.* **3**, e39 (2007).
52. Eden, E., Navon, R., Steinfeld, I., Lipson, D. & Yakhini, Z. GOrilla: a tool for discovery and visualization of enriched GO terms in ranked gene lists. *BMC Bioinformatics* **10**, 48 (2009).
53. Khambhati, A. N. et al. Recurring functional interactions predict network architecture of interictal and ictal states in neocortical epilepsy. *eNeuro* **4**, 1–18 (2017).
54. Chapeton, J. I., Inati, S. K. & Zaghloul, K. A. Stable functional networks exhibit consistent timing in the human brain. *Brain* **140**, 628–640 (2017).
55. Solomon, E. et al. Widespread theta synchrony and high-frequency desynchronization underlies enhanced cognition. *Nat. Commun.* **8**, 1704 (2017).
56. Power, J. D., Barnes, K. A., Snyder, A. Z., Schlaggar, B. L. & Petersen, S. E. Spurious but systematic correlations in functional connectivity MRI networks arise from subject motion. *NeuroImage* **59**, 2142–2154 (2012).
57. Clune, J., Mouret, J.-B. & Lipson, H. The evolutionary origins of modularity. *Proc. R. Soc. B* **280**, 20122863 (2013).
58. Mantini, D., Perrucci, M. G., Del Gratta, C. D., Romani, G. L. & Corbetta, M. Electrophysiological signatures of resting state networks in the human brain. *Proc. Natl Acad. Sci. USA* **104**, 13170–13175 (2007).
59. Marzetti, L. et al. Frequency specific interactions of MEG resting state activity within and across brain networks as revealed by the multivariate interaction measure. *NeuroImage* **79**, 172–183 (2013).
60. Battiston, F., Nicosia, V., Chavez, M. & Latora, V. Multilayer motif analysis of brain networks. *Chaos* **27**, 047404 (2017).
61. Kucyi, A. et al. Intracranial electrophysiology reveals reproducible intrinsic functional connectivity within human brain networks. *J. Neurosci.* **38**, 4230–4242 (2018).
62. Conner, C. R., Ellmore, T. M., Pieters, T. A., DiSano, M. A. & Tandon, N. Variability of the relationship between electrophysiology and BOLD-fMRI across cortical regions in humans. *J. Neurosci.* **31**, 12855–12865 (2011).
63. Goense, J. B. M. & Logothetis, N. K. Neurophysiology of the BOLD fMRI signal in awake monkeys. *Curr. Biol.* **18**, 631–640 (2008).
64. Winawer, J. et al. Asynchronous broadband signals are the principal source of the BOLD response in human visual cortex. *Curr. Biol.* **23**, 1145–1153 (2013).
65. Miller, K. J., Honey, C. J., Hermes, D., Rao, R. P. N. & Ojemann, J. G. Broadband changes in the cortical surface potential track activation of functionally diverse neuronal populations. *NeuroImage* **85**, 711–720 (2014).
66. Hinne, M. et al. The missing link: predicting connectomes from noisy and partially observed tract tracing data. *PLoS Comput. Biol.* **13**, e1005374 (2017).
67. Lo, R. Y., Jagust, W. J. & Alzheimer's Disease Neuroimaging Initiative. Predicting missing biomarker data in a longitudinal study of Alzheimer disease. *Neurology* **78**, 1376–1382 (2012).
68. Henle, C. et al. First long term in vivo study on subdurally implanted micro-ECoG electrodes, manufactured with a novel laser technology. *Biomed. Micro.* **13**, 59–68 (2011).
69. Lu, L., Pan, L., Zhou, T., Zhang, Y. C. & Stanley, H. E. Toward link predictability of complex networks. *Proc. Natl Acad. Sci. USA* **112**, 2325–2330 (2015).
70. Pan, L., Zhou, T., Lu, L. & Hu, C. K. Predicting missing links and identifying spurious links via likelihood analysis. *Sci. Rep.* **6**, 22955 (2016).
71. Margulies, D. S. et al. Situating the default-mode network along a principal gradient of macroscale cortical organization. *Proc. Natl Acad. Sci. USA* **113**, 12574–12579 (2016).
72. Honey, C. J., Kötter, R., Breakspear, M. & Sporns, O. Network structure of cerebral cortex shapes functional connectivity on multiple time scales. *Proc. Natl Acad. Sci. USA* **104**, 10240–10245 (2007).
73. Hermundstad, A. M. et al. Structural foundations of resting-state and task-based functional connectivity in the human brain. *Proc. Natl Acad. Sci. USA* **110**, 6169–6174 (2013).
74. Betzel, R. F. et al. Multi-scale community organization of the human structural connectome and its relationship with resting-state functional connectivity. *Netw. Sci.* **1**, 353–373 (2013).
75. Rubinov, M., Ypma, R. J., Watson, C. & Bullmore, E. T. Wiring cost and topological participation of the mouse brain connectome. *Proc. Natl Acad. Sci. USA* **112**, 10032–10037 (2015).
76. Gaiteri, C., Ding, Y., French, B., Tseng, G. C. & Sibille, E. Beyond modules and hubs: the potential of gene coexpression networks for investigating molecular mechanisms of complex brain disorders. *Genes Brain Behav.* **13**, 13–24 (2014).
77. Pezawas, L. et al. 5-HTTLPR polymorphism impacts human cingulate–amygdala interactions: a genetic susceptibility mechanism for depression. *Nat. Neurosci.* **8**, 828–834 (2005).
78. Meyer-Lindenberg, A. et al. Neural mechanisms of genetic risk for impulsivity and violence in humans. *Proc. Natl Acad. Sci. USA* **103**, 6269–6274 (2006).
79. Goulas A., et al. Cytoarchitectonic similarity is a wiring principle of the human connectome. Preprint at https://www.biorxiv.org/content/10.1101/068254v1 (2016).
80. Glasser, M. F. et al. A multi-modal parcellation of human cerebral cortex. *Nature* **536**, 171–178 (2016).
81. Baaré, W. F. C. et al. Quantitative genetic modeling of variation in human brain morphology. *Cereb. Cortex* **11**, 816–824 (2001).
82. Whitaker, K. J. et al. Adolescence is associated with genomically patterned consolidation of the hubs of the human brain connectome. *Proc. Natl Acad. Sci. USA* **113**, 9105–9110 (2016).
83. Hawrylycz, M. J. et al. An anatomically comprehensive atlas of the adult human brain transcriptome. *Nature* **489**, 391–399 (2012).
84. Chu, C. J. et al. EEG functional connectivity is partially predicted by underlying white matter connectivity. *NeuroImage* **108**, 23–33 (2015).
85. Birn, R. M., Diamond, J. B., Smith, M. A. & Bandettini, P. A. Separating respiratory-variation-related fluctuations from neuronal-activity-related fluctuations in fMRI. *NeuroImage* **31**, 1536–1548 (2006).
86. Liu, T. T. Neurovascular factors in resting-state functional MRI. *NeuroImage* **80**, 339–348 (2013).
87. Hagmann, P. et al. Mapping the structural core of human cerebral cortex. *PLoS Biol.* **6**, e159 (2008).
88. Deco, G., Jirsa, V. K. & McIntosh, A. R. Emerging concepts for the dynamical organization of resting-state activity in the brain. *Nat. Rev. Neurosci.* **12**, 43–56 (2011).
89. Jones, A. R., Overly, C. C. & Sunkin, S. M. The Allen Brain Atlas: 5 years and beyond. *Nat. Rev. Neurosci.* **10**, 821–828 (2009).
90. Sunkin, S. M. et al. Allen Brain Atlas: an integrated spatio-temporal portal for exploring the central nervous system. *Nucleic acids Res.* **41**, D996–D1008 (2013).
91. Thomas, C. et al. Anatomical accuracy of brain connections derived from diffusion MRI tractography is inherently limited. *Proc. Natl Acad. Sci. USA* **111**, 16574–16579 (2014).
92. Reveley, C. et al. Superficial white matter fiber systems impede detection of long-range cortical connections in diffusion MR tractography. *Proc. Natl Acad. Sci. USA* **112**, E2820–E2828 (2015).
93. Bassett, D. S. et al. Dynamic reconfiguration of human brain networks during learning. *Proc. Natl Acad. Sci. USA* **108**, 7641–7646 (2011).
94. Zhou, D., Thompson, W. K. & Siegle, G. MATLAB toolbox for functional connectivity. *NeuroImage* **47**, 1590–1607 (2009).
95. Kitzbichler, M. G., Smith, M. L., Christensen, S. R. & Bullmore, E. Broadband criticality of human brain network synchronization. *PLoS Comput. Biol.* **5**, e1000314 (2009).
96. Betzel, R. F. et al. Synchronization dynamics and evidence for a repertoire of network states in resting EEG. *Front. Comput. Neurosci.* **6**, 74 (2012).
97. Smith, S. M. et al. Network modelling methods for fMRI. *NeuroImage* **54**, 875–891 (2011).
98. Park, H.-J. & Friston, K. Structural and functional brain networks: from connections to cognition. *Science* **342**, 1238411 (2013).
99. He, B. J., Snyder, A. Z., Zempel, J. M., Smyth, M. D. & Raichle, M. E. Electrophysiological correlates of the brain's intrinsic large-scale functional architecture. *Proc. Natl Acad. Sci. USA* **105**, 16039–16044 (2008).
100. Kramer, M. A., Eden, U. T., Cash, S. S. & Kolaczyk, E. D. Network inference with confidence from multivariate time series. *Phys. Rev. E* **79**, 061916 (2009).
101. Owen, L. L. W. & Manning, J. R. Towards human super EEG. Preprint at https://www.biorxiv.org/content/10.1101/121020v1 (2017).
102. Rosset, A., Spadola, L. & Ratib, O. OsiriX: an open-source software for navigating in multidimensional DICOM images. *J. Digit. Imaging* **17**, 205–216 (2004).
103. Betzel, R. F., Gu, S., Medaglia, J. D., Pasqualetti, F. & Bassett, D. S. Optimally controlling the human connectome: the role of network topology. *Sci. Rep.* **6**, 30770 (2016).
104. Betzel, R. F. et al. The modular organization of human anatomical brain networks: accounting for the cost of wiring. *Netw. Neurosci.* **1**, 42–68 (2017).
105. Betzel, R. F., Medaglia, J. D. & Bassett, D. S. Diversity of meso-scale architecture in human and non-human connectomes. *Nat. Commun.* **9**, 346 (2018).
106. Mišić, B. et al. Cooperative and competitive spreading dynamics on the human connectome. *Neuron* **86**, 1518–1529 (2015).
107. Roberts, J. A., Perry, A., Roberts, G., Mitchell, P. B. & Breakspear, M. Consistency-based thresholding of the human connectome. *NeuroImage* **145**, 118–129 (2017).
108. Jones, D. K., Knösche, T. R. & Turner, R. White matter integrity, fiber count, and other fallacies: the do's and don'ts of diffusion MRI. *NeuroImage* **73**, 239–254 (2013).

109. Jenkinson, M., Beckmann, C. F., Behrens, T. E. J., Woolrich, M. W. & Smith, S. M. FSL. *NeuroImage* **62**, 782–790 (2012).
110. Greve, D. N. & Fischl, B. Accurate and robust brain image alignment using boundary-based registration. *NeuroImage* **48**, 63–72 (2009).
111. Zhang, Y., Brady, M. & Smith, S. Segmentation of brain MR images through a hidden Markov random field model and the expectation–maximization algorithm. *IEEE Trans. Med. Imaging* **20**, 45–57 (2001).
112. Jenkinson, M., Bannister, P., Brady, M. & Smith, S. Improved optimization for the robust and accurate linear registration and motion correction of brain images. *NeuroImage* **17**, 825–841 (2002).
113. Murphy, K., Birn, R. M., Handwerker, D. A., Jones, T. B. & Bandettini, P. A. The impact of global signal regression on resting state correlations: are anti-correlated networks introduced? *NeuroImage* **44**, 893–905 (2009).
114. Power, J. D., Plitt, M., Laumann, T. O. & Martin, A. Sources and implications of whole-brain fMRI signals in humans. *NeuroImage* **146**, 609–625 (2017).
115. Simpson, S. L., Moussa, M. N. & Laurienti, P. J. An exponential random graph modeling approach to creating group-based representative whole-brain connectivity networks. *NeuroImage* **60**, 1117–1126 (2012).
116. Bazzi, M. et al. Community detection in temporal multilayer networks, with an application to correlation networks. *Multiscale Model. Simul.* **14**, 1–41 (2016).
117. Betzel, R. F. & Bassett, D. S. Multi-scale brain networks. *NeuroImage* **160**, 73–83 (2017).
118. Iturria-Medina, Y., Sotero, R. C., Canales-Rodrí, E. J., Alemán-Gómez, Y. & Melie-García, L. Studying the human brain anatomical network via diffusion-weighted MRI and graph theory. *NeuroImage* **40**, 1064–1076 (2008).
119. Wirsich, J. et al. Whole-brain analytic measures of network communication reveal increased structure–function correlation in right temporal lobe epilepsy. *NeuroImage Clin.* **11**, 707–718 (2016).

Acknowledgements

The resting-state fMRI and diffusion imaging data collection was funded by the Army Research Office through contract number W911NF-14-1-0679 awarded to D.S.B. R.F.B. and J.S. were supported by grants awarded to D.S.B., including awards from the John D. and Catherine T. MacArthur Foundation, Alfred P. Sloan Foundation, ISI Foundation, Paul G. Allen Family Foundation, Army Research Laboratory (W911NF-10-2-0022), Army Research Office (Bassett-W911NF-14-1-0679, Grafton-W911NF-16-1-0474 and DCIST-W911NF-17-2-0181), Office of Naval Research, National Institute of Mental Health (2-R01-DC-009209-11, R01-MH112847, R01-MH107235 and R21-M MH-106799), National Institute of Child Health and Human Development (1R01HD086888-01), National Institute of Neurological Disorders and Stroke (R01 NS099348) and National Science Foundation (BCS-1441502, BCS-1430087, NSF PHY-1554488 and BCS-1631550). A.E.K. was supported by a grant awarded to D.S.B. from the Army Research Laboratory through contract number W911NF-10-2-0022. J.D.M. acknowledges support from the National Institute of Health (award 1-DP5-OD021352). This content is solely the responsibility of the authors and does not necessarily represent the official views of any of the funding agencies. We also thank M. Kahana and the group associated with the DARPA Restoring Active Memory programme, who were responsible for collecting and publicly sharing the ECoG data used in this paper.

Author contributions

R.F.B. and D.S.B. designed the study, performed all analyses and wrote the initial draft of the manuscript. J.D.M., A.E.K. and J.S. contributed to and processed the MRI data. D.R.S. helped with the Gene Ontology analysis. All authors wrote the final draft of the manuscript.

Competing interests

The authors declare no competing Interests.

Additional information

Supplementary information is available for this paper at https://doi.org/10.1038/s41551-019-0404-5.

Reprints and permissions information is available at www.nature.com/reprints.

Correspondence and requests for materials should be addressed to D.S.B.

Publisher's note: Springer Nature remains neutral with regard to jurisdictional claims in published maps and institutional affiliations.

nature research

Corresponding author(s): Danielle Bassett

Last updated by author(s): Mar 5, 2019

Reporting Summary

Nature Research wishes to improve the reproducibility of the work that we publish. This form provides structure for consistency and transparency in reporting. For further information on Nature Research policies, see Authors & Referees and the Editorial Policy Checklist.

Statistics

For all statistical analyses, confirm that the following items are present in the figure legend, table legend, main text, or Methods section.

n/a	Confirmed	
☐	☒	The exact sample size (*n*) for each experimental group/condition, given as a discrete number and unit of measurement
☐	☒	A statement on whether measurements were taken from distinct samples or whether the same sample was measured repeatedly
☐	☒	The statistical test(s) used AND whether they are one- or two-sided *Only common tests should be described solely by name; describe more complex techniques in the Methods section.*
☐	☒	A description of all covariates tested
☐	☒	A description of any assumptions or corrections, such as tests of normality and adjustment for multiple comparisons
☐	☒	A full description of the statistical parameters including central tendency (e.g. means) or other basic estimates (e.g. regression coefficient) AND variation (e.g. standard deviation) or associated estimates of uncertainty (e.g. confidence intervals)
☐	☒	For null hypothesis testing, the test statistic (e.g. *F*, *t*, *r*) with confidence intervals, effect sizes, degrees of freedom and *P* value noted *Give P values as exact values whenever suitable.*
☒	☐	For Bayesian analysis, information on the choice of priors and Markov chain Monte Carlo settings
☒	☐	For hierarchical and complex designs, identification of the appropriate level for tests and full reporting of outcomes
☐	☒	Estimates of effect sizes (e.g. Cohen's *d*, Pearson's *r*), indicating how they were calculated

Our web collection on statistics for biologists contains articles on many of the points above.

Software and code

Policy information about availability of computer code

Data collection	The data has been made available upon request by the Restoring Active Memory (RAM) consortium (http://memory.psych.upenn.edu/RAM_Public_Data). OsiriX DICOM viewer (http://osirix-viewer.com) was used to digitize electrode locations, which were subsequently mapped to locations in standardized space. This process had already been implemented by the time we accessed the dataset.
Data analysis	Network construction, analysis, and predictive modeling was carried out by using custom MATLAB code. All code is available upon request. Gene ontology analysis was performed by using GOrilla (http://cbl-gorilla.cs.technion.ac.il). This software is not associated with any explicit version number, although the most recent update to GOrilla software was made on March 8, 2013 (http://cbl-gorilla.cs.technion.ac.il/news.html).

For manuscripts utilizing custom algorithms or software that are central to the research but not yet described in published literature, software must be made available to editors/reviewers. We strongly encourage code deposition in a community repository (e.g. GitHub). See the Nature Research guidelines for submitting code & software for further information.

Data

Policy information about availability of data

All manuscripts must include a data availability statement. This statement should provide the following information, where applicable:

- Accession codes, unique identifiers, or web links for publicly available datasets
- A list of figures that have associated raw data
- A description of any restrictions on data availability

The authors declare that the main data supporting the results in this study are available within the paper and its Supplementary Information. All source data collected from the subjects are available upon request via http://memory.psych.upenn.edu/RAM_Public_Data.

Field-specific reporting

Please select the one below that is the best fit for your research. If you are not sure, read the appropriate sections before making your selection.

☒ Life sciences ☐ Behavioural & social sciences ☐ Ecological, evolutionary & environmental sciences

For a reference copy of the document with all sections, see nature.com/documents/nr-reporting-summary-flat.pdf

Life sciences study design

All studies must disclose on these points even when the disclosure is negative.

Sample size	The population consisted of 86 individuals with medication resistant epilepsy.
Data exclusions	We excluded 3 subjects whose data did not include electrode coordinates. As a result, we analyzed data from 83 individuals.
Replication	We did not have a replication dataset. However, to ensure robustness of modeling results, we performed two cross-validation analyses: the first involved fitting model parameters to 82 subjects and using fit model to predict connectivity of held-out subject. We also fit the model using data from a single subject and used the model to predict connectivity of remaining 82 subjects.
Randomization	There was no group allocation in this study.
Blinding	There was no group allocation in this study.

Reporting for specific materials, systems and methods

We require information from authors about some types of materials, experimental systems and methods used in many studies. Here, indicate whether each material, system or method listed is relevant to your study. If you are not sure if a list item applies to your research, read the appropriate section before selecting a response.

Materials & experimental systems

n/a	Involved in the study
☒	☐ Antibodies
☒	☐ Eukaryotic cell lines
☒	☐ Palaeontology
☒	☐ Animals and other organisms
☐	☒ Human research participants
☒	☐ Clinical data

Methods

n/a	Involved in the study
☒	☐ ChIP-seq
☒	☐ Flow cytometry
☐	☒ MRI-based neuroimaging

Human research participants

Policy information about studies involving human research participants

Population characteristics	Subjects had medication resistant epilepsy.
Recruitment	Patients were being monitored as part of clinical treatment of epilepsy and were recruited to participate in the study.
Ethics oversight	Research protocols were approved by the Institutional Review Boards of participating centers and hospitals (Columbia University, Dartmouth College, Emory University, Thomas Jefferson University, Mayo Clinic, National Institutes of Health, University of Texas Southwestern, Lawrence Livermore National Labs, University of Pennsylvania).

Note that full information on the approval of the study protocol must also be provided in the manuscript.

Magnetic resonance imaging

Experimental design

Design type	We analyzed three different MRI datasets; resting functional MRI; and two diffusion MRI data (one reported in the main Article, the other reported in the Supplementary Information).
Design specifications	Functional MRI data was collected at rest.
Behavioral performance measures	n/a

Acquisition

Imaging type(s): Functional and diffusion MRI

Field strength: 3T

Sequence & imaging parameters: Resting fMRI: TR = 1500 ms; TE = 30 ms; Flip Angle = 60 degrees; FOV = 19.2 cm; resolution 3 mm isotropic

Diffusion MRI (see below)

Area of acquisition: Whole-brain

Diffusion MRI ☒ Used ☐ Not used

Parameters: Diffusion MRI (main text): Q5 half-shell; 257 directions; b-value = 5000; TR = 5 s; TE = 138 ms;

Diffusion MRI (Supplementary Methods): 730 directions; maximum b-value = 5010; TR = 4300 ms; TE = 102 ms; 21 interspersed b0 images.

Preprocessing

Preprocessing software: Functional MRI processed with FSL using FEAT (v.6.0). Skull-stripping with BET; Motion correction with MCFLIRT; slice-timing correction (interleaved); spatial smoothing with 6mm 3D Gaussian kernel; high-pass filter to reduce low-frequency drift.

Normalization: EPI unwarping with fieldmaps. Images registered to standard space using FLIRT. Subject images co-registered to anatomical (T1) images using BBR.

Normalization template: MNI-152 via 12-parameter linear transform.

Noise and artifact removal: White-matter time series, CSF time series, and 18 translational/rotational parameters (estimated using MCFLIRT) included as regressors.

Volume censoring: None

Statistical modeling & inference

Model type and settings: n/a

Effect(s) tested: n/a

Specify type of analysis: ☒ Whole brain ☐ ROI-based ☐ Both

Statistic type for inference (See Eklund et al. 2016): n/a

Correction: n/a

Models & analysis

n/a	Involved in the study
☐	☒ Functional and/or effective connectivity
☐	☒ Graph analysis
☒	☐ Multivariate modeling or predictive analysis

Functional and/or effective connectivity: Functional connectivity measured as inter-regional correlations. Structural connectivity between regions i and j measured as streamline count divided by geometric mean of i's and j's total volume.

Graph analysis: Graph analyses were carried out on weighted networks. In the case of functional connectivity, we used a modified version of the modularity heuristic to detect modules. The modification allowed modularity maximization to be applied to networks with missing connection weights and involved setting elements of the modularity matrix to zero if no connection was present.

Using the structural connectivity, we computed the measure 'search information', which quantifies the information needed (in units of bits) to follow the shortest path from region i to j. We repeated this for all pairs of brain regions.